Acta Mech 225, 1649–1672 (2014)
DOI 10.1007/s00707-013-1017-9

X. S. Sun · V. B. C. Tan · Y. Chen · L. B. Tan · R. K. Jaiman · T. E. Tay

Stress analysis of multi-layered hollow anisotropic composite cylindrical structures using the homogenization method

Received: 19 April 2013 / Revised: 16 August 2013 / Published online: 7 November 2013

Abstract This paper presents a general and efficient stress analysis strategy for hollow composite cylindrical structures consisting of multiple layers of different anisotropic materials subjected to different loads. Cylindrical material anisotropy and various loading conditions are considered in the stress analysis. The general stress solutions for homogenized hollow anisotropic cylinders subjected to pressure, axial force, torsion, shear and bending are presented with explicit formulations under typical force and displacement boundary conditions. The stresses and strains in a layer of the composite cylindrical structures are obtained from the solutions of homogenized hollow cylinders with effective material properties and discontinuous layer material properties. Effective axial, torsional, bending and coupling stiffness coefficients taking into account material anisotropy are also determined from the strain solutions for the hollow composite cylindrical structures. Examples show that the material anisotropy may have significant effects on the effective stiffness coefficients in some cases. The stress analysis method is demonstrated with an example of stress analysis of a 22-layer composite riser, and the results are compared with numerical solutions. This method is efficient for stress analysis of thin-walled or moderately thick-walled hollow composite cylindrical structures with various multiple layers of different materials or arbitrary fiber angles because no explicit interfacial continuity parameters are required. It provides an efficient and easy-to-use analysis tool for assessing hollow composite cylindrical structures in engineering applications.

1 Introduction

Hollow cylindrical structures, e.g., tubes, pipes, vessels, risers, etc., are widely utilized in the modern oil and gas industry. These structures usually have thin or moderately thick walls and are subjected to certain loads such as pressure, tension, torsion, bending and shear. The design of these kinds of structures usually requires that they have high strength but light weight. Therefore, composite materials with the advantages of better mechanical performances and light specific weight are increasingly used in these cylindrical structures. The composite cylindrical structures can be considered as coaxially bonded cylinders consisting of multiple layers of different materials. Under a load, the stress distributions in the composite cylindrical structures are complicated due to the geometrical curvature, material anisotropy and discontinuity in the structures. The elastic equilibrium of a homogenous hollow cylinder with arbitrary anisotropy has been comprehensively investigated by Lekhnitskii [1] using the stress function method. The well-known Lekhnitskii formalism was hence established and extensively used in solving various anisotropic elastic problems including stress analysis of heterogeneous composite structures. In Lekhnitskii formalism, equilibrated stress functions and

X. S. Sun · V. B. C. Tan (✉) · Y. Chen · L. B. Tan · R. K. Jaiman · T. E. Tay
Department of Mechanical Engineering, National University of Singapore,
9 Engineering Drive 1, Singapore 117576, Singapore
E-mail: mpetanbc@nus.edu.sg
Tel.: +65-65168088
Fax: +65-67791459

strain compatibility equations form a system of partial differential equations. Then the stress solutions are obtained from the stress functions obtained from the partial differential equations. Based on the stress functions in Lekhnitskii formalism, Jolicoeur and Cardou [2] investigated coaxial hollow circular orthotropic cylinders subjected to bending, tensile and torsion loads. These formulations were also used by Chouchaoui et al. [3,4] to analyze a laminated cylindrical tube subjected to tensile, torsion, bending, internal and external pressure loading conditions. Wild and Vickers [5] extended Lekhnitskii's work to develop a stress and deformation analysis method based on classical laminated plate theory for filament-wound cylindrical shells subjected to combined centrifugal, pressure and axial loads. A similar method was also presented by Parnas and Katirci [6] to design and predict the behavior of fiber-reinforced composite pressure vessels. Verijenko et al. [7] adopted Lekhnitskii's stress function approach to obtain exact elasticity solutions for both open-ended and closed-ended laminated circular cylinders subjected to internal, external and interlaminar pressures. This approach was also used by Xia et al. [8] to analyze multi-layered filament-wound composite pipes under bending load.

Another popular approach for the analysis of anisotropic elasticity is the well-known Stroh formalism which was originated by Stroh [9] and then thoroughly developed by Ting [10]. Unlike Lekhnitskii formalism, Stroh formalism makes use of compatible displacements and equilibrium equations to form a system of partial differential equations. The displacement solutions are then obtained from the partial differential equations. From this displacement-based approach, Kollár et al. [11,12] presented a stress analysis of composite cylinders subjected to hydrothermal and mechanical loads. Bhaskar and Varadan [13] derived an exact three-dimensional elasticity solution for cylindrical bending of simply supported laminated anisotropic cylindrical shells subjected to transverse loading. Xia et al. [14,15] presented an exact elastic solution for stresses and deformations of filament-wound composite pipes under internal pressure and thermomechanical loading. Similar methods were also used by Bakaiyan et al. [16] and Calhoglu et al. [17] for investigating filament-wound composite pipes under thermal loads. Tarn and Wang [18,19] extended the Stroh formalism by considering both displacement and stress variables in the equilibrium equations and proposed a state space method to analyze composite tubes under extension, torsion, bending, shear and pressure.

In all the above works based on either Lekhnitskii formalism or Stroh formalism for analyzing multi-layered composite cylindrical structures, interfacial continuity parameters determined from displacement and stress continuity between layers have to be required explicitly in the solutions. The solutions therefore become complicated and cumbersome with many interfacial continuity parameters to be determined for composite cylindrical structures with many layers of different materials or fiber angles. Furthermore, new sets of parameters must be re-calculated with each different loading condition, layup or material change for multi-layered composite cylindrical structures. Besides these analytical methods, an alternative numerical approach for stress analysis of composite cylindrical structures is the well-known finite element method (FEM). For multi-layered hollow composite structures, the finite element (FE) models can be based on either multi-layered solid elements or composite elements. In the FE model with multi-layered solid elements, each layer is modeled with at least one solid element through the thickness and therefore a large amount of solid elements are required. This model can give accurate numerical solutions with finer mesh and even low-order elements, but it needs a longer computational time due to the large number of elements. In the FE model with composite elements, all adjacent layers having the same material, but different fiber angles are usually built with one element through the thickness and then these layers are modeled through different section points (or integration points) with different fiber orientations in the element [20–22]. This model is suitable for composite structures with many adjacent layers having the same material. However, with increasing number of layers, higher order elements (e.g., 15-order elements [21]) and more through-thickness integration points are required in order to accurately capture the stresses and strains in each layer. As higher order elements are not used in most applications, multiple through-thickness low-order (linear or quadratic) composite elements are commonly employed instead [23]. Models with low-order composite elements are based on linear strain compatibility assumptions and thus unable to predict through-thickness normal and shear stresses or strains accurately. Nevertheless, this deficiency may be overcome by increasing the number of composite elements in the thickness direction.

This paper presents an efficient stress analysis method for hollow composite cylindrical structures with multiple layers of different anisotropic materials subjected to various loading conditions including internal and external pressures, axial force, torsion, shears and bending moments. The stress analysis follows the Lekhnitskii formalism and is based on a homogenization method. The solutions of homogenized hollow cylinders with effective material properties and discontinuous layer material properties are used to determine the stresses and strains in a layer of hollow composite cylindrical structures. In the current work, the stress solutions of homogenized hollow cylinders are presented with explicit formulations under various boundary conditions. Based on the stress analysis, effective axial, torsional, bending and coupling stiffness coefficients taking into

account material anisotropy are also derived for the hollow composite cylindrical structures. The effects of material anisotropy on the effective stiffness coefficients are discussed through examples. The application of the stress analysis method is demonstrated with an example, and the results are compared with numerical solutions from FEM.

The paper is organized as follows. In Sect. 2, general elastic solutions of multi-layered hollow composite cylindrical structures are presented. Section 3 presents stress solutions of homogenized hollow cylinders under various loading conditions, employing the stress function method. In Sect. 4, the homogenization method for the stress analysis of multi-layered hollow composite cylindrical structures and the determination of the effective material properties are presented, and the effective stiffness coefficients are derived. In Sect. 5, two examples are provided to demonstrate the evaluation of the effective stiffness coefficients for anisotropic cylinders and the application of the proposed stress analysis method. Finally, some conclusions are drawn in Sect. 6.

2 General elastic solutions of multi-layered hollow composite cylindrical structures

A hollow composite cylindrical structure considered in this paper generally consists of multiple layers of different materials, and these layers can be considered as coaxial hollow cylinders. The basic geometrical parameters for the composite cylindrical structure are length L, inner radius a and outer radius b as shown in the cylindrical coordinate system in Fig. 1. The total number of layers is n; r_i and r_{i+1} are the inner and outer radius of the (i)th layer, respectively. Dimensionless parameters are defined as $c_i = r_i/b$ and $c_{i+1} = r_{i+1}/b$, with $c_1 = c = a/b$ and $c_{n+1} = 1$. The stacking sequence is from inner to outer layers. The material of a layer in the composite cylindrical structure is homogenously isotropic or anisotropic, which corresponds to an isotropic layer or a composite layer. A composite layer is typically made of orthotropic fiber-reinforced materials and fabricated by filament-winding technology. The reinforced fibers in a layer have the same winding angle, or the helix angle $\varphi^{(i)}$, as shown in Fig. 1b. Therefore, the material in the composite layer can be considered as a monoclinic anisotropy in the cylindrical coordinate system, and the axis of anisotropy coincides with z-axis. Isotropy and orthotropy can be considered as special cases of the monoclinic anisotropy.

The following assumptions are adopted in the present analysis: (i) perfectly bonded layers, (ii) small and elastic strains and (iii) constant loads, stresses and strains along z-axis, implying that the stresses and strains are functions of r and θ only. In the cylindrical coordinate system, if the r direction is taken as the normal to the plane of elastic symmetry and temperature is neglected, the equilibrium equation, geometrical equation and constitutive equation of the (i)th layer of the composite cylindrical structure can be, respectively, written as:

$$\nabla_1 \boldsymbol{\sigma}^{(i)} + \boldsymbol{f}_b^{(i)} = \mathbf{0}, \tag{2.1}$$

$$\boldsymbol{\varepsilon}^{(i)} = \nabla_1' \boldsymbol{u}^{(i)}, \tag{2.2}$$

$$\boldsymbol{\varepsilon}^{(i)} = S^{(i)} \boldsymbol{\sigma}^{(i)} \quad \text{or} \quad \boldsymbol{\sigma}^{(i)} = \boldsymbol{D}^{(i)} \boldsymbol{\varepsilon}^{(i)}. \tag{2.3}$$

The superscript (i) denotes the (i)th layer; ∇_1 and ∇_1' are the differential operator matrices of the first order defined, respectively, in Eqs. (A.1) and (A.2) in the "Appendix"; $\boldsymbol{\sigma}^{(i)}$, $\boldsymbol{\varepsilon}^{(i)}$, $\boldsymbol{u}^{(i)}$ and $\boldsymbol{f}_b^{(i)}$ are the vectors of

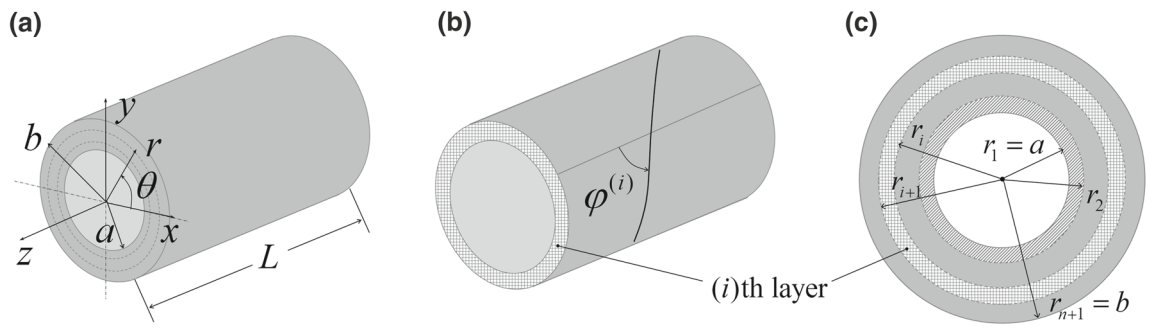

Fig. 1 A multi-layered hollow composite cylindrical structure with **a** basic geometrical parameters, **b** fiber angle in a composite layer and **c** stacking sequence

stress, strain, displacement and body force density of the (i)th layer, respectively, and

$$\begin{cases} \boldsymbol{\sigma}^{(i)} = \left[\sigma_r^{(i)} \quad \sigma_\theta^{(i)} \quad \sigma_z^{(i)} \quad \tau_{\theta z}^{(i)} \quad \tau_{rz}^{(i)} \quad \tau_{r\theta}^{(i)} \right]^{\mathrm{T}}, \\ \boldsymbol{\varepsilon}^{(i)} = \left[\varepsilon_r^{(i)} \quad \varepsilon_\theta^{(i)} \quad \varepsilon_z^{(i)} \quad \gamma_{\theta z}^{(i)} \quad \gamma_{rz}^{(i)} \quad \gamma_{r\theta}^{(i)} \right]^{\mathrm{T}}, \end{cases} \tag{2.4}$$

$$\boldsymbol{u}^{(i)} = \left[u_r^{(i)} \; u_\theta^{(i)} \; u_z^{(i)} \right]^{\mathrm{T}}, \tag{2.5}$$

$$\boldsymbol{f}_b^{(i)} = \left[f_r^{(i)} \; f_\theta^{(i)} \; f_z^{(i)} \right]^{\mathrm{T}} = \left[-\frac{\partial W^{(i)}}{\partial r} \; -\frac{\partial W^{(i)}}{r\partial\theta} \; -\frac{\partial W^{(i)}}{\partial z} \right]^{\mathrm{T}}, \tag{2.6}$$

$$\boldsymbol{S}^{(i)} = \begin{bmatrix} s_{11}^{(i)} & s_{12}^{(i)} & s_{13}^{(i)} & s_{14}^{(i)} & 0 & 0 \\ s_{12}^{(i)} & s_{22}^{(i)} & s_{23}^{(i)} & s_{24}^{(i)} & 0 & 0 \\ s_{13}^{(i)} & s_{23}^{(i)} & s_{33}^{(i)} & s_{34}^{(i)} & 0 & 0 \\ s_{14}^{(i)} & s_{24}^{(i)} & s_{34}^{(i)} & s_{44}^{(i)} & 0 & 0 \\ 0 & 0 & 0 & 0 & s_{55}^{(i)} & s_{56}^{(i)} \\ 0 & 0 & 0 & 0 & s_{56}^{(i)} & s_{66}^{(i)} \end{bmatrix}, \tag{2.7}$$

$$\boldsymbol{D}^{(i)} = \left(\boldsymbol{S}^{(i)} \right)^{-1} = \begin{bmatrix} d_{11}^{(i)} & d_{12}^{(i)} & d_{13}^{(i)} & d_{14}^{(i)} & 0 & 0 \\ d_{12}^{(i)} & d_{22}^{(i)} & d_{23}^{(i)} & d_{24}^{(i)} & 0 & 0 \\ d_{13}^{(i)} & d_{23}^{(i)} & d_{33}^{(i)} & d_{34}^{(i)} & 0 & 0 \\ d_{14}^{(i)} & d_{24}^{(i)} & d_{34}^{(i)} & d_{44}^{(i)} & 0 & 0 \\ 0 & 0 & 0 & 0 & d_{55}^{(i)} & d_{56}^{(i)} \\ 0 & 0 & 0 & 0 & d_{56}^{(i)} & d_{66}^{(i)} \end{bmatrix} \tag{2.8}$$

where $W^{(i)}$ is the body force potential; $s_{jl}^{(i)}$ and $d_{jl}^{(i)} (j, l = 1, 2, 3, 4, 5, 6)$ are the material compliance and stiffness components of the (i)th layer, respectively; the reduced material compliance components $\beta_{jl}^{(i)}$ can be calculated as [1]:

$$\beta_{jl}^{(i)} = s_{jl}^{(i)} - s_{j3}^{(i)} s_{l3}^{(i)} / s_{33}^{(i)}. \tag{2.9}$$

From Lekhnitskii formalism [1], the general stress solutions of the composite cylindrical structure can be expressed by the stress functions as:

$$\begin{cases} \sigma_r^{(i)} = \frac{\partial F^{(i)}}{r\partial r} + \frac{\partial^2 F^{(i)}}{r^2 \partial\theta^2} + W^{(i)}, \quad \sigma_\theta^{(i)} = \frac{\partial^2 F^{(i)}}{\partial r^2} + W^{(i)}, \\ \tau_{r\theta}^{(i)} = \frac{\partial F^{(i)}}{r^2\partial\theta} - \frac{\partial^2 F^{(i)}}{r\partial r\partial\theta}, \quad \tau_{rz}^{(i)} = \frac{\partial \Psi^{(i)}}{r\partial\theta}, \quad \tau_{\theta z}^{(i)} = -\frac{\partial \Psi^{(i)}}{\partial r}, \\ \sigma_z^{(i)} = \frac{1}{s_{33}^{(i)}} \left(C_1^{(i)} r\cos\theta + C_2^{(i)} r\sin\theta + C_0^{(i)} - s_{13}^{(i)}\sigma_r^{(i)} - s_{23}^{(i)}\sigma_\theta^{(i)} - s_{34}^{(i)}\tau_{\theta z}^{(i)} \right) \end{cases} \tag{2.10}$$

where $C_0^{(i)}$, $C_1^{(i)}$ and $C_2^{(i)}$ are constants to be determined from boundary conditions and interfacial continuity conditions; $F^{(i)}$ and $\Psi^{(i)}$ are the stress functions determined from solving the following system of partial differential equations:

$$\begin{bmatrix} L_4'^{(i)} & L_3'^{(i)} \\ L_3''^{(i)} & L_2'^{(i)} \end{bmatrix} \begin{bmatrix} F^{(i)} \\ \Psi^{(i)} \end{bmatrix} = \begin{bmatrix} N_1^{(i)} \\ N_2^{(i)} \end{bmatrix}. \tag{2.11}$$

In Eq. (2.11), $L_2'^{(i)}$, $L_3'^{(i)}$, $L_3''^{(i)}$ and $L_4'^{(i)}$ are the differential operators of the second, third and fourth orders defined in Eq. (A.3) in the "Appendix"; $N_1^{(i)}$ and $N_2^{(i)}$ are two functions of r and θ written as:

$$\begin{cases} N_1^{(i)} = \frac{s_{13}^{(i)} - s_{23}^{(i)}}{r s_{33}^{(i)}} \left(2C_1^{(i)} \cos\theta + 2C_2^{(i)} \sin\theta\right) + N_{b,1}^{(i)}, \\ N_2^{(i)} = \frac{s_{34}^{(i)}}{r s_{33}^{(i)}} \left(2C_1^{(i)} r \cos\theta + 2C_2^{(i)} r \sin\theta + C_0^{(i)}\right) - \frac{2\Upsilon^{(i)}}{b} + N_{b,2}^{(i)}, \end{cases} \tag{2.12}$$

$$\begin{cases} N_{b,1}^{(i)} = \left(\beta_{12}^{(i)} + \beta_{22}^{(i)}\right) \frac{\partial f_r^{(i)}}{\partial r} + \left(\beta_{11}^{(i)} + \beta_{12}^{(i)}\right) \frac{\partial f_\theta^{(i)}}{r \partial \theta} - \left(\beta_{11}^{(i)} - \beta_{12}^{(i)} - 2\beta_{22}^{(i)}\right) \frac{f_r^{(i)}}{r}, \\ N_{b,2}^{(i)} = -\left(\beta_{14}^{(i)} + \beta_{24}^{(i)}\right) \left(f_r^{(i)} + \frac{W^{(i)}}{r}\right) \end{cases} \tag{2.13}$$

where $\Upsilon^{(i)}$ is a constant to be determined from boundary conditions and interfacial continuity conditions.

With the aid of Eqs. (2.2) and (2.3), the general displacement solutions of the composite cylindrical structure can be expressed as:

$$\begin{cases} u_r^{(i)} = -z^2 \left(C_1^{(i)} \cos\theta + C_2^{(i)} \sin\theta\right)/2 + U_r^{(i)} + u_r'^{(i)}, \\ u_\theta^{(i)} = -z^2 \left(C_2^{(i)} \cos\theta - C_1^{(i)} \sin\theta\right)/2 + U_\theta^{(i)} + \Upsilon^{(i)} r z / b + u_\theta'^{(i)}, \\ u_z^{(i)} = z \left(C_1^{(i)} r \cos\theta + C_2^{(i)} r \sin\theta + C_0^{(i)}\right) + U_z^{(i)} + u_z'^{(i)} \end{cases} \tag{2.14}$$

where $U_r^{(i)}$, $U_\theta^{(i)}$ and $U_z^{(i)}$ are determined from integration of Eq. (2.2); $u_r'^{(i)}$, $u_\theta'^{(i)}$ and $u_z'^{(i)}$ are three rigid-body displacements.

It may be noted that Eq. (2.14) can also be obtained through the geometrical equations and strain compatibility equations [24], which indicates that the expressions in Eq. (2.14) are independent of physical properties of materials.

Under given loading conditions, the solutions from Eqs. (2.10) and (2.14) for each layer contain a series of constants or parameters, which need to be determined from the following boundary conditions:

$$\boldsymbol{u} = \bar{\boldsymbol{u}} \quad \text{on } \Gamma_u, \quad \boldsymbol{F}_s = \bar{\boldsymbol{F}}_s \quad \text{on } \Gamma_{F_s}, \tag{2.15}$$

and the continuity conditions at the interfaces between two adjacent layers:

$$\begin{cases} \sigma_r^{(i)} = \sigma_r^{(i+1)}, \quad \tau_{rz}^{(i)} = \tau_{rz}^{(i+1)}, \quad \tau_{r\theta}^{(i)} = \tau_{r\theta}^{(i+1)} \\ u_r^{(i)} = u_r^{(i+1)}, \quad u_\theta^{(i)} = u_\theta^{(i+1)}, \quad u_z^{(i)} = u_z^{(i+1)} \end{cases} \quad \text{at } \Gamma_s^{(i)}, \tag{2.16}$$

where $\bar{\boldsymbol{u}}$ and Γ_u are prescribed generalized displacement and the corresponding boundary; $\bar{\boldsymbol{F}}_s$ and Γ_{F_s} are applied generalized force and the corresponding boundary; $\Gamma_s^{(i)}$ is the interface between the (i)th and $(i+1)$th layers.

It can be seen that the determination of the parameters in the solutions depends on different loading conditions and the interfacial continuity conditions. Therefore, the total number of parameters to be determined will increase significantly with larger number of layers of the composite cylindrical structures. Furthermore, these parameters have to be re-calculated with the number of layers change. There are also similar issues in Stroh formalism (e.g., the solutions in [14,15]). This paper presents a homogenization method to circumvent the cumbersome determination of the interfacial continuity parameters. The solutions of homogenized hollow anisotropic cylinders under given loading conditions are used in this method, and they are to be determined from Eqs. (2.10) and (2.11).

3 Stress solutions for a homogenized hollow anisotropic cylinder

Consider a homogenized hollow cylinder with length L, inner radius a, outer radius b and the ratio $c = a/b$ in a cylindrical coordinate system (r, θ, z) as shown in Fig. 1a. Unless otherwise stated, the variables and parameters without superscript "(i)" are hereafter in the context of homogeneity. Loading conditions considered in the stress analysis include internal pressure p, external pressure q, axial force P, torsion (twisting moment) M_t,

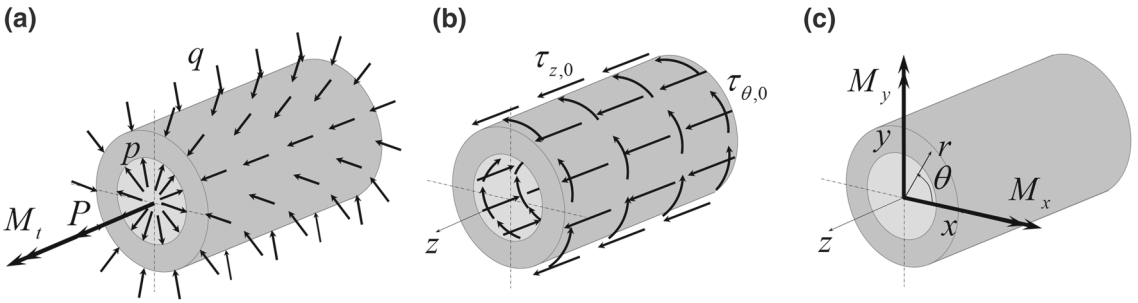

Fig. 2 A hollow cylinder under typical loads of **a** pressure, axial force and torsion, **b** axial and in-plane shears and **c** bending moments

axial (anti-plane) shear $\tau_{z,0}$, in-plane shear $\tau_{\theta,0}$ and bending moments M_x and M_y. The body force is neglected (i.e., $W = 0$). These loads are categorized into three groups as shown in Fig. 2a–c, respectively. For the first and second group loadings with pressure, axial force, torsion and shears, the stress distributions on the cross section are axisymmetrical and are functions of r only. For the third group loadings with bending moments, the stress distributions on the cross section are more complicated and are functions of both r and θ.

The solutions of a homogenous hollow anisotropic cylinder under loading conditions in Fig. 2a, c were discussed by Lekhnitskii [1], and stress solutions for some special cases were obtained using the stress function method. However, some constants in Lekhnitskii's solutions are not determined, and there are some misprints in Lekhnitskii's formulations (41.13) and (43.4) [1]. This paper presents the stress solutions with explicit formulations from Eqs. (2.10) and (2.11) under the loading conditions as shown in Fig. 2, and all the constants required in the solutions are determined from the corresponding boundary conditions. Prescribed displacement boundary conditions are also discussed.

3.1 Pressure, axial force, torsion and shears

Under internal pressure p, external pressure q, axial force P, torsion (twisting moment) M_t, axial shear $\tau_{z,0}$ and in-plane shear $\tau_{\theta,0}$, the constants C_1 and C_2 in Eq. (2.12) are zero due to the axisymmetry. By defining $C = C_0/s_{33}$, F and Ψ can be solved analytically from Eq. (2.11) as:

$$\begin{cases} F(r,\theta) = \sum_{j=1}^{2} \frac{C_j^* r^{k_j+1}}{(k_j+1)b^{k_j-1}} + \frac{\Upsilon\mu_1 r^3}{3b} + \frac{C\delta_1 r^2}{2} + C_1' b^2\theta, \\ \Psi(r,\theta) = \sum_{j=1}^{2} \frac{C_j^* g_{k_j} r^{k_j}}{k_j b^{k_j-1}} - \frac{\Upsilon\mu_2 r^2}{2b} + C\delta_2 r + C_2' b\theta \end{cases} \tag{3.1}$$

where $C_1^*, C_2^*, C_1', C_2', C$ and Υ are constants to be determined; $k_j, g_{k_j} (j = 1, 2)$, μ_1, μ_2, δ_1 and δ_2 are parameters defined as:

$$k_j = (-1)^{j+1} \sqrt{\frac{\beta_{11}\beta_{44} - \beta_{14}^2}{\beta_{22}\beta_{44} - \beta_{24}^2}}, \tag{3.2}$$

$$g_{k_j} = \left(\beta_{14} + k_j\beta_{24}\right)/\beta_{44}, \tag{3.3}$$

$$\begin{cases} \mu_1 = \frac{\beta_{14}-2\beta_{24}}{(4\beta_{22}-\beta_{11})\beta_{44}+(\beta_{14}^2-4\beta_{24}^2)}, \\ \mu_2 = \frac{4\beta_{22}-\beta_{11}}{(4\beta_{22}-\beta_{11})\beta_{44}+(\beta_{14}^2-4\beta_{24}^2)}, \end{cases} \tag{3.4}$$

$$\begin{cases} \delta_1 = \frac{(s_{13}-s_{23})\beta_{44}-s_{34}(\beta_{14}-\beta_{24})}{(\beta_{22}-\beta_{11})\beta_{44}+(\beta_{14}^2-\beta_{24}^2)}, \\ \delta_2 = \frac{(s_{13}-s_{23})(\beta_{14}+\beta_{24})+s_{34}(\beta_{22}-\beta_{11})}{(\beta_{22}-\beta_{11})\beta_{44}+(\beta_{14}^2-\beta_{24}^2)}. \end{cases} \tag{3.5}$$

It can be verified that the parameters μ_1, μ_2, δ_1 and δ_2 fulfill the two identities $\mu_1(\beta_{14} + 2\beta_{24}) + \mu_2\beta_{44} = 1$ and $\delta_1(\beta_{14} + \beta_{24}) + s_{34} - \delta_2\beta_{44} = 0$. The parameters s_{jl} and $\beta_{jl} (j, l = 1, 2, 3, 4, 5, 6)$ in Eqs. (3.2)–(3.5) are

the effective normal and reduced material compliance components of the homogenized cylinder, respectively. Then the general axisymmetrical stress distributions on the cross section of the homogenized hollow anisotropic cylinder can be obtained from Eqs. (2.10) and (3.1) as:

$$\begin{cases} \sigma_r = \sum_{j=1}^{2} C_j^* \rho^{k_j-1} + \Upsilon\mu_1\rho + C\delta_1, \\ \sigma_\theta = \sum_{j=1}^{2} C_j^* k_j \rho^{k_j-1} + 2\Upsilon\mu_1\rho + C\delta_1, \\ \tau_{\theta z} = -\sum_{j=1}^{2} C_j^* g_{k_j} \rho^{k_j-1} + \Upsilon\mu_2\rho - C\delta_2, \\ \sigma_z = C - (s_{13}\sigma_r + s_{23}\sigma_\theta + s_{34}\tau_{\theta z})/s_{33}, \\ \tau_{rz} = C_2'/\rho, \\ \tau_{r\theta} = C_1'/\rho^2 \end{cases} \tag{3.6}$$

where $\rho = r/b$.

The constants C_1^*, C_2^*, C and Υ in Eq. (3.6) are determined from the following boundary conditions:

$$\sigma_r|_{\rho=c} = -p, \quad \sigma_r|_{\rho=1} = -q, \tag{3.7}$$

$$\int_0^{2\pi}\int_a^b \sigma_z r \mathrm{d}r\mathrm{d}\theta = P, \quad \int_0^{2\pi}\int_a^b \tau_{\theta z} r^2 \mathrm{d}r\mathrm{d}\theta = M_t. \tag{3.8}$$

From Eqs. (3.6) and (3.7), the constants C_j^* $(j = 1, 2)$ can be obtained as:

$$C_j^* = p_{k_j}^* - C\delta_1 c_{k_j,1}^* - \Upsilon\mu_1 c_{k_j,2}^* \tag{3.9}$$

where

$$p_{k_j}^* = \frac{pc^{k_j+1} - q}{1 - c^{2k_j}}, \quad c_{k_j,l}^* = \frac{1 - c^{k_j+l}}{1 - c^{2k_j}}, \quad (j, l = 1, 2), \tag{3.10}$$

By substituting Eq. (3.9) into Eq. (3.6), the remaining two constants C and Υ can be determined from Eq. (3.8). After lengthy and cumbersome algebraic manipulations, C and Υ can be explicitly solved from Eq. (3.8) as:

$$C = \frac{\Sigma_2 P}{2\pi b^2 \Sigma_0} - \frac{\Sigma_1 M_t}{2\pi b^3 \Sigma_0} + C_p, \quad \Upsilon = \frac{B_1 M_t}{2\pi b^3 \Sigma_0} - \frac{B_2 P}{2\pi b^2 \Sigma_0} + \Upsilon_p \tag{3.11}$$

where

$$\begin{cases} C_p = \frac{1}{\Sigma_0}\sum_{j=1}^{2} p_{k_j}^* \left(e_{k_j} K_{k_j,1}\Sigma_2 - g_{k_j} K_{k_j,2}\Sigma_1\right), \\ \Upsilon_p = \frac{1}{\Sigma_0}\sum_{j=1}^{2} p_{k_j}^* \left(g_{k_j} K_{k_j,2} B_1 - e_{k_j} K_{k_j,1} B_2\right), \end{cases} \tag{3.12}$$

$$\Sigma_0 = B_1\Sigma_2 - B_2\Sigma_1, \tag{3.13}$$

$$\begin{cases} B_1 = \frac{1-\delta^*}{2}\left(1 - c^2\right) + \delta_1 \sum_{j=1}^{2} e_{k_j} K_{k_j,1} c_{k_j,1}^*, \\ B_2 = -\frac{\delta_2}{3}\left(1 - c^3\right) + \delta_1 \sum_{j=1}^{2} g_{k_j} K_{k_j,2} c_{k_j,1}^*, \end{cases} \tag{3.14}$$

$$\begin{cases} \Sigma_1 = -\frac{\mu^*}{3}\left(1 - c^3\right) + \mu_1 \sum_{j=1}^{2} e_{k_j} K_{k_j,1} c_{k_j,2}^*, \\ \Sigma_2 = \frac{\mu_2}{4}\left(1 - c^4\right) + \mu_1 \sum_{j=1}^{2} g_{k_j} K_{k_j,2} c_{k_j,2}^*, \end{cases} \tag{3.15}$$

$$\delta^* = (\delta_1 s_{13} + \delta_1 s_{23} - \delta_2 s_{34})/s_{33}, \tag{3.16}$$

$$\mu^* = (\mu_1 s_{13} + 2\mu_1 s_{23} + \mu_2 s_{34})/s_{33}, \tag{3.17}$$

$$e_{k_j} = \left(s_{13} + k_j s_{23} - g_{k_j} s_{34}\right)/s_{33}, \quad (j = 1, 2), \tag{3.18}$$

$$K_{k_j,l} = \begin{cases} \ln(1/c), & \text{if } l = -k_j \\ \frac{1-c^{k_j+l}}{k_j+l}, & \text{if } l \neq -k_j \end{cases}, \quad (j, l = 1, 2). \tag{3.19}$$

The constants C_1' and C_2' in Eq. (3.6) are determined from the axial and in-plane shear boundary conditions. For example, if the axial and in-plane shears $\tau_{\theta,0}$ and $\tau_{z,0}$ are acting on the external surface of the cylinder as shown in Fig. 2b, i.e.,:

$$\tau_{rz}|_{\rho=1} = \tau_{z,0}, \quad \tau_{r\theta}|_{\rho=1} = \tau_{\theta,0}, \tag{3.20}$$

then C_1' and C_2' can be determined as:

$$C_1' = \tau_{\theta,0}, \quad C_2' = \tau_{z,0}. \tag{3.21}$$

It can be seen that the two through-thickness shear stresses τ_{rz} and $\tau_{r\theta}$ in Eq. (3.6) are independent of materials. It may be noted that Eq. (3.6) is similar to the solution given by Lekhnitskii [1] under pressures, tension and torsion except for several misprints in Lekhnitskii's equations (41.13), i.e., a minus sign (−) in σ_θ is mistaken for a plus sign (+), and $\tau_{\theta z}$ is misprinted as $\tau_{r\theta}$. The parameter μ_2 in Eq. (3.4) is also mistaken for $-\mu_2$ in Lekhnitskii's equations (41.1).

If the loading conditions are axial, and in-plane shears only as shown in Fig. 2b, we have $C_1^* = C_2^* = C = \Upsilon = 0$ from Eqs. (3.9)–(3.12), and the stress solutions are simplified as:

$$\begin{cases} \sigma_r = \sigma_\theta = \sigma_z = \tau_{\theta z} = 0 \\ \tau_{rz} = C_2'/\rho, \quad \tau_{r\theta} = C_1'/\rho^2 \end{cases}. \tag{3.22}$$

If the loading conditions are pressures, tension and torsion only as shown in Fig. 2a, we have $C_1' = C_2' = 0$ and then $\tau_{rz} = \tau_{r\theta} = 0$. It can be seen that under axial and in-plane shear loadings the corresponding shear stresses are not coupled with other deformations for monoclinic materials, i.e., the shear loadings cause anti-plane and in-plane shear deformations only and vice versa.

If the hollow cylinder is orthotropic, i.e., $s_{14} = s_{24} = s_{34} = s_{56} = 0$, we have $g_{k_j} = \delta_2 = \mu_1 = \mu^* = 0$, $B_2 = \Sigma_1 = 0$ and

$$k_j = (-1)^{j+1}\sqrt{\beta_{11}/\beta_{22}}, \tag{3.23}$$

$$\delta_1 = \frac{s_{13} - s_{23}}{\beta_{22} - \beta_{11}}, \quad \mu_2 = \frac{1}{\beta_{44}} = \frac{1}{s_{44}}, \quad \Sigma_2 = \frac{\mu_2}{4}\left(1 - c^4\right). \tag{3.24}$$

Other nonzero parameters (B_1, δ^*, e_{k_j}) for the orthotropic case have the same formulations as those in Eqs. (3.14), (3.16) and (3.18) except for some zero terms with s_{34}. Then Eq. (3.11) is simplified as:

$$C = \frac{P}{2\pi b^2 B_1} + \frac{1}{B_1}\sum_{j=1}^{2} p_{k_j}^* e_{k_j} K_{k_j,1}, \quad \Upsilon = \frac{2M_t}{\pi b^3 \mu_2 \left(1 - c^4\right)}, \tag{3.25}$$

and the stresses σ_r, σ_θ, σ_z and $\tau_{\theta z}$ in Eq. (3.6) are simplified as:

$$\begin{cases} \sigma_r = \sum_{j=1}^{2}\left(p_{k_j}^* - C\delta_1 c_{k_j,1}^*\right)\rho^{k_j - 1} + C\delta_1, \\ \sigma_\theta = \sum_{j=1}^{2}\left(p_{k_j}^* - C\delta_1 c_{k_j,1}^*\right)k_j\rho^{k_j - 1} + C\delta_1, \\ \sigma_z = C - (s_{13}\sigma_r + s_{23}\sigma_\theta)/s_{33}, \\ \tau_{\theta z} = \Upsilon\mu_2\rho. \end{cases} \tag{3.26}$$

It can be seen that the normal stresses σ_r, σ_θ, σ_z are caused only by internal pressure p, external pressure q and axial force P, and the shear stress $\tau_{\theta z}$ is caused only by torsion M_t for the orthotropic case. Furthermore, if the hollow cylinder is isotropic, i.e., $s_{11} = s_{22} = s_{33}$ and $s_{12} = s_{13} = s_{23}$, we have $k_1 = -k_2 = 1$, $\delta_1 = \delta^* = 0$ and $B_1 = \left(1 - c^2\right)/2$. Then the radial and hoop stresses (σ_r and σ_θ) in Eq. (3.26) can be further simplified as the well-known Lamè's formula which is independent of materials for the isotropic case.

If $C = \Upsilon = 0$ and $\tau_{\theta,0} = \tau_{z,0} = 0$, Eq. (3.6) is reduced to the solution due to internal and external pressures in the plane strain problem. In this case, the axial force P and twisting moment M_t due to the plane strain constraints are solved from Eq. (3.11) or (3.25) with $C = \Upsilon = 0$.

3.2 Bending moments

Stress distributions on the cross section of a homogenized hollow cylinder having cylindrical anisotropy due to bending moments M_x and M_y, as shown in Fig. 2c, are more complicated, and all the six stress components are usually nonzero. The constants C_0 and Υ in Eq. (2.12) are zero due to the pure bending problem. By defining $C_1 = -s_{33}M_y/I_y$ and $C_2 = s_{33}M_x/I_x$, F and Ψ can be solved analytically from Eq. (2.11) using the method of separating variables as:

$$\begin{cases} F(r,\theta) = \left(\frac{M_x}{I_x}\sin\theta - \frac{M_y}{I_y}\cos\theta\right)\left(\sum_{j=1}^{4}\frac{H_j r^{m_j+1}}{m_j b^{m_j-2}} + \frac{\lambda_1 r^3}{2}\right), \\ \Psi(r,\theta) = \left(\frac{M_x}{I_x}\sin\theta - \frac{M_y}{I_y}\cos\theta\right)\left(\sum_{j=1}^{4}\frac{H_j g_{m_j} r^{m_j}}{b^{m_j-2}} + \lambda_2 r^2\right), \end{cases} \tag{3.27}$$

where I_x, I_y and $H_j (j = 1, 2, 3, 4)$ are constants to be determined; m_j, $g_{m_j} (j = 1, 2, 3, 4)$, λ_1 and λ_2 are parameters defined as:

$$\begin{cases} m_j = (-1)^{j+1}\sqrt{\frac{-\delta_b+\sqrt{\delta_b^2-4\delta_a\delta_c}}{2\delta_a}}, & \text{if } j = 1, 2, \\ m_j = (-1)^{j+1}\sqrt{\frac{-\delta_b-\sqrt{\delta_b^2-4\delta_a\delta_c}}{2\delta_a}}, & \text{if } j = 3, 4, \end{cases} \tag{3.28}$$

$$g_{m_j} = \begin{cases} \frac{\beta_{24}m_j^3+(\beta_{14}+\beta_{24})m_j^2-\beta_{56}m_j}{\beta_{44}m_j^2-\beta_{55}}, & \text{if } m_j^2 \neq \beta_{55}/\beta_{44}, \\ 0, & \text{if } m_j^2 = \beta_{55}/\beta_{44}, \end{cases} \tag{3.29}$$

$$\lambda_1 = \frac{2s_{34}\Lambda_{22} - (s_{13}-s_{23})\Lambda_{12}}{\Lambda_{11}\Lambda_{22}-\Lambda_{12}\Lambda_{21}}, \quad \lambda_2 = \frac{(s_{13}-s_{23})\Lambda_{11} - 2s_{34}\Lambda_{21}}{\Lambda_{11}\Lambda_{22}-\Lambda_{12}\Lambda_{21}}, \tag{3.30}$$

$$\begin{cases} \delta_a = \beta_{22}\beta_{44} - \beta_{24}^2, \\ \delta_b = (\beta_{14}+\beta_{24})^2 + 2\beta_{24}\beta_{56} - \beta_{44}(\beta_{11}+2\beta_{12}+\beta_{22}+\beta_{66}) - \beta_{22}\beta_{55}, \\ \delta_c = \beta_{55}(\beta_{11}+2\beta_{12}+\beta_{22}+\beta_{66}) - \beta_{56}^2, \end{cases} \tag{3.31}$$

$$\begin{cases} \Lambda_{11} = -2\beta_{14} - 6\beta_{24} + \beta_{56}, \quad \Lambda_{12} = 4\beta_{44} - \beta_{55}, \\ \Lambda_{21} = -\beta_{11} - 2\beta_{12} + 3\beta_{22} - \beta_{66}, \quad \Lambda_{22} = 2\beta_{14} - 2\beta_{24} + \beta_{56}. \end{cases} \tag{3.32}$$

By substituting Eq. (3.27) into Eq. (2.10), the stress solutions of the homogenized hollow anisotropic cylinder due to the bending moments can be obtained as:

$$\begin{cases} \sigma_r = \left(\frac{M_x}{I_x}\sin\theta - \frac{M_y}{I_y}\cos\theta\right)\left(\sum_{j=1}^{4} H_j\rho^{m_j-2} + \lambda_1\right)r, \\ \sigma_\theta = \left(\frac{M_x}{I_x}\sin\theta - \frac{M_y}{I_y}\cos\theta\right)\left[\sum_{j=1}^{4} H_j\left(m_j+1\right)\rho^{m_j-2} + 3\lambda_1\right]r, \\ \tau_{\theta z} = -\left(\frac{M_x}{I_x}\sin\theta - \frac{M_y}{I_y}\cos\theta\right)\left(\sum_{j=1}^{4} H_j g_{m_j} m_j\rho^{m_j-2} + 2\lambda_2\right)r, \\ \tau_{rz} = \left(\frac{M_x}{I_x}\cos\theta + \frac{M_y}{I_y}\sin\theta\right)\left(\sum_{j=1}^{4} H_j g_{m_j}\rho^{m_j-2} + \lambda_2\right)r, \\ \tau_{r\theta} = -\left(\frac{M_x}{I_x}\cos\theta + \frac{M_y}{I_y}\sin\theta\right)\left(\sum_{j=1}^{4} H_j\rho^{m_j-2} + \lambda_1\right)r, \\ \sigma_z = \left(\frac{M_x}{I_x}\sin\theta - \frac{M_y}{I_y}\cos\theta\right)r - \frac{1}{s_{33}}\left(s_{13}\sigma_r + s_{23}\sigma_\theta + s_{34}\tau_{\theta z}\right). \end{cases} \tag{3.33}$$

The constants $H_j (j = 1, 2, 3, 4)$ in Eq. (3.33) are determined from the boundary conditions $\sigma_r = \tau_{r\theta} = \tau_{rz} = 0$ when $r = a$ and $r = b$ (free surfaces) and can be written as:

$$\begin{bmatrix} H_1 \\ H_2 \\ H_3 \\ H_4 \end{bmatrix} = -\begin{bmatrix} c^{m_1-2} & c^{m_2-2} & c^{m_3-2} & c^{m_4-2} \\ 1 & 1 & 1 & 1 \\ g_{m_1}c^{m_1-2} & g_{m_2}c^{m_2-2} & g_{m_3}c^{m_3-2} & g_{m_4}c^{m_4-2} \\ g_{m_1} & g_{m_2} & g_{m_3} & g_{m_4} \end{bmatrix}^{-1}\begin{bmatrix} \lambda_1 \\ \lambda_1 \\ \lambda_2 \\ \lambda_2 \end{bmatrix}, \tag{3.34}$$

The constants I_x and I_y in Eq. (3.33) are determined, respectively, from the following two equilibrium conditions:

$$\int_0^{2\pi}\int_a^b \sigma_z r^2 \sin\theta \mathrm{d}r\mathrm{d}\theta = M_x, \quad \int_0^{2\pi}\int_a^b \sigma_z r^2 \cos\theta \mathrm{d}r\mathrm{d}\theta = -M_y. \tag{3.35}$$

For hollow circular cylindrical structures, we have $I_x = I_y = I$. By substituting σ_z in Eq. (3.33) into Eq. (3.35), the constants I_x and I_y can be solved as:

$$I_x = I_y = I = \frac{\pi b^4}{4}\left(1-c^4\right)\left(1-\lambda^*\right) - \pi b^4 \sum_{j=1}^{4} H_j m_j^* K_{m_j}, \tag{3.36}$$

where

$$\lambda^* = \left(s_{13}\lambda_1 + 3s_{23}\lambda_1 - 2s_{34}\lambda_2\right)/s_{33}, \tag{3.37}$$

$$m_j^* = \left[s_{13} + s_{23}\left(m_j+1\right) - s_{34} g_{m_j} m_j\right]/s_{33}, \tag{3.38}$$

$$K_{m_j} = \begin{cases} \ln\left(1/c\right), & \text{if } m_j = -2 \\ \frac{1-c^{m_j+2}}{m_j+2}, & \text{if } m_j \neq -2 \end{cases} \quad (j = 1, 2, 3, 4). \tag{3.39}$$

The maximum values of stresses $\sigma_r, \sigma_\theta, \sigma_z, \tau_{\theta z}$ occur at $\theta = 90 + \theta_{c1}$, and the maximum values of stresses $\tau_{r\theta}, \tau_{rz}$ occur at $\theta = 90 - \theta_{c2}$, where $\theta_{c1} = \arctan M_y/M_x$ and $\theta_{c2} = \arctan M_x/M_y$. If the hollow cylinder is orthotropic, we have $g_{m_j} = \lambda_2 = 0$, $\tau_{\theta z} = \tau_{rz} = 0$ and

$$\begin{cases} m_j = (-1)^{j+1}\sqrt{1 + (\beta_{11} + 2\beta_{12} + \beta_{66})/\beta_{22}}, & \text{if } j = 1, 2, \\ m_j = (-1)^{j+1}\sqrt{\beta_{55}/\beta_{44}}, & \text{if } j = 3, 4, \end{cases} \tag{3.40}$$

$$\lambda_1 = \frac{a_{23} - a_{13}}{\beta_{11} + 2\beta_{12} + \beta_{66} - 3\beta_{22}}. \tag{3.41}$$

Then the constants $H_j (j = 1, 2, 3, 4)$ for the orthotropic case are simplified as:

$$\begin{bmatrix} H_1 \\ H_2 \end{bmatrix} = -\begin{bmatrix} c^{m_1-2} & c^{m_2-2} \\ 1 & 1 \end{bmatrix}^{-1} \begin{bmatrix} \lambda_1 \\ \lambda_1 \end{bmatrix}, \quad H_3 = H_4 = 0. \tag{3.42}$$

Furthermore, if the hollow cylinder is isotropic, we have $m_1 = -m_2 = 2$, $m_3 = -m_4 = 1$, $\lambda_1 = \lambda^* = H_j = 0$, $I = \pi b^4\left(1-c^4\right)/4$, $\sigma_r = \sigma_\theta = \tau_{\theta z} = \tau_{rz} = \tau_{r\theta} = 0$ and $\sigma_z = \left(M_x \sin\theta - M_y \cos\theta\right) r/I$, which implies that the bending moments cause only the axial stress σ_z for the isotropic case.

It can be verified that the reduced solutions in Eqs. (3.33), (3.36), (3.40) and (3.41) for the orthotropic hollow cylinder under the bending moment M_x are the same as those given by Lekhnitskii [1] in his equations (43.16)–(43.18) and (43.11), respectively.

3.3 Prescribed displacement boundary conditions

If the boundary conditions are known forces or stresses (force loading), the stress solutions can be directly obtained from Eqs. (3.6) and (3.33). For the first group loading conditions in Fig. 2a, if the boundary conditions are known displacements or strains (prescribed displacement), these displacement-type boundary conditions can be converted to force-type boundary conditions, and then the stress can be calculated from the converted force, stress or moment with Eq. (3.6). According to Eqs. (2.3) and (3.6), the axial strain ε_z, shear strain $\gamma_{\theta z}$ and radial displacement u_r for the first group loading conditions can be obtained as:

$$\varepsilon_z = Cs_{33}, \quad \gamma_{\theta z} = \Upsilon\rho, \tag{3.43}$$

$$u_r = b\left(\sum_{j=1}^{2} f_{k_j}^p(\rho) p_{k_j}^* + f_P(\rho)P + f_M(\rho)M_t\right) \tag{3.44}$$

where $f_{k_j}^p(\rho)$, $f_P(\rho)$ and $f_M(\rho)$ are functions of ρ only, and

$$\begin{cases} f_{k_j}^p(\rho) = \rho\left(\beta_{k_j}\rho^{k_j-1} + \beta_j^p\right), \quad (j=1,2), \\ f_P(\rho) = \frac{\rho}{2\pi b^2 \Sigma_0}\left(\beta_\rho^* \Sigma_2 - \delta_\rho^* B_2\right), \quad f_M(\rho) = \frac{\rho}{2\pi b^3 \Sigma_0}\left(\delta_\rho^* B_1 - \beta_\rho^* \Sigma_1\right), \end{cases} \tag{3.45}$$

$$\beta_{k_j} = \left(\beta_{11} + k_j\beta_{12} - g_{k_j}\beta_{14}\right)/k_j, \tag{3.46}$$

$$\beta_j^p = \frac{1}{\Sigma_0}\left[\beta_\rho^*\left(e_{k_j}K_{k_j,1}\Sigma_2 - g_{k_j}K_{k_j,2}\Sigma_1\right) + \delta_\rho^*\left(g_{k_j}K_{k_j,2}B_1 - e_{k_j}K_{k_j,1}B_2\right)\right], \tag{3.47}$$

$$\beta_\rho^* = \delta_1\left(\beta_{11}+\beta_{12}\right) - \delta_2\beta_{14} + s_{13} - \delta_1\sum_{j=1}^{2} c_{k_j,1}^*\beta_{k_j}\rho^{k_j-1}, \tag{3.48}$$

$$\delta_\rho^* = \frac{\rho}{2}\left[\mu_1\left(\beta_{11}+2\beta_{12}\right) + \mu_2\beta_{14}\right] - \mu_1\sum_{j=1}^{2} c_{k_j,2}^*\beta_{k_j}\rho^{k_j-1}, \tag{3.49}$$

and other parameters can be found in Eqs. (3.2)–(3.5) and (3.10)–(3.19).

For the first group loading conditions as shown in Fig. 2a, there are generally three typical types of displacement boundary conditions: (i) prescribed radial deformations $u_{r,a}^0$ and/or $u_{r,b}^0$ on the internal and/or external surfaces, respectively, (ii) prescribed axial strain ε_z^0 (or displacement $u_{z,0}^0$ at one end of the cylinder) and (iii) prescribed in-plane rotation θ_L^0 (on the cross section) at one end and relative to the other end of the cylinder, and the corresponding shear strain $\gamma_{\theta z}^0$ due to this in-plane rotation is $\gamma_{\theta z}^0 = r\theta_L^0/L$. These three types of displacement boundary conditions will cause corresponding internal and/or external pressure p_0 and/or q_0, axial force P_0 and twisting moment $M_{t,0}$, respectively. These converted forces and moments due to any one or combinations of these prescribed displacement boundary conditions can be found from Eqs. (3.43) and (3.44). Several important and common cases for these prescribed displacement boundary conditions and corresponding converted forces and moments are as follows:

1. prescribed radial displacements on both internal and external surfaces, $u_{r,a}^0$and $u_{r,b}^0$:

$$\begin{bmatrix} p_0 \\ q_0 \end{bmatrix} = -\begin{bmatrix} c^{k_1-1} & c^{k_2-1} \\ 1 & 1 \end{bmatrix}\begin{bmatrix} f_{k_1}^p(c) & f_{k_2}^p(c) \\ f_{k_1}^p(1) & f_{k_2}^p(1) \end{bmatrix}^{-1}\begin{bmatrix} u_{r,a}^0/b - f_0(c) \\ u_{r,b}^0/b - f_0(1) \end{bmatrix} \tag{3.50}$$

where

$$f_0(\rho) = f_P(\rho)P + f_M(\rho)M_t; \tag{3.51}$$

2. prescribed radial displacement on the internal surface only, $u_{r,a}^0$:

$$p_0 = \left(\frac{u_{r,a}^0}{b} - f_0(c) + q\sum_{j=1}^{2}\frac{f_{k_j}^p(c)}{1-c^{2k_j}}\right) \Bigg/ \sum_{j=1}^{2}\frac{c^{k_j+1}f_{k_j}^p(c)}{1-c^{2k_j}}; \tag{3.52}$$

3. prescribed radial displacement on the external surface only, $u_{r,b}^0$:

$$q_0 = \left(\frac{u_{r,b}^0}{b} - f_0(1) + p\sum_{j=1}^{2}\frac{c^{k_j+1}f_{k_j}^p(1)}{c^{2k_j}-1}\right) \Bigg/ \sum_{j=1}^{2}\frac{f_{k_j}^p(1)}{c^{2k_j}-1}; \tag{3.53}$$

4. prescribed axial strain only, ε_z^0:

$$P_0 = 2\pi b^2\left[\frac{\Sigma_0}{\Sigma_2}\cdot\frac{\varepsilon_z^0}{s_{33}} + \sum_{j=1}^{2} p_{k_j}^*\left(\frac{\Sigma_1}{\Sigma_2}g_{k_j}K_{k_j,2} - e_{k_j}K_{k_j,1}\right)\right] + \frac{\Sigma_1}{\Sigma_2}\cdot\frac{M_t}{b}; \tag{3.54}$$

5. prescribed in-plane rotation (on the cross section of one end) only, θ_L^0:

$$M_{t,0} = 2\pi b^3 \left[\frac{\Sigma_0}{B_1} \cdot \frac{b\theta_L^0}{L} + \sum_{j=1}^{2} p_{k_j}^* \left(\frac{B_2}{B_1} e_{k_j} K_{k_j,1} - g_{k_j} K_{k_j,2} \right) \right] + \frac{B_2}{B_1} Pb. \tag{3.55}$$

For the third group loading conditions with bending moments as shown in Fig. 2c, if the cylinder is long and $L \gg b$, there will be significant deflections off z axis. In this case, a typical prescribed displacement condition is the prescribed maximum deflection or the prescribed rotation at one end of the cylinder. The displacements or deflections u_x and u_y under bending moments M_x and M_y can be obtained from Eq. (2.14) as:

$$u_x = \frac{M_y z^2}{2E_z I_y} + f_x(r,\theta) r + u' + \omega_y' z_x, \quad u_y = -\frac{M_x z^2}{2E_z I_x} + f_y(r,\theta) r + u_y' - \omega_x' z, \tag{3.56}$$

where $-L \le z \le 0$ and $E_z = 1/s_{33}$; $f_x(r,\theta)$ and $f_y(r,\theta)$ are functions of r and θ; u_x', u_y', ω_x' and ω_y' are rigid translations and rotations of the cylinder about x and y axes, respectively.

If $L \gg b$, then $f_x(r)r \ll u_x$ and $f_y(r)r \ll u_y$, and they can be neglected from the deflection equations defined in Eq. (3.56). This also means that the nominal deflection based on the neutral axis ($r = 0$) is considered for the long cylinder. For simplicity, one end of the cylinder is fixed, i.e., $u_x = u_y = 0$ at $z = 0$ as shown in Fig. 2c, then $u_x' = u_y' = 0$. The constants ω_x' and ω_y' can be obtained from the boundary conditions of the other end of the cylinder ($z = -L$). An important case is that $u_x = u_y = 0$ at $z = -L$ and the deflections and rotations (in radians) can be written as:

$$u_x = \frac{M_y}{2E_z I_y} \left(z^2 + Lz \right), \quad u_y = -\frac{M_x}{2E_z I_x} \left(z^2 + Lz \right), \tag{3.57}$$

$$\tan \omega_x = -\frac{\mathrm{d}u_y}{\mathrm{d}z} = \frac{M_x}{2E_z I_x} (2z + L), \quad \tan \omega_y = \frac{\mathrm{d}u_x}{\mathrm{d}z} = \frac{M_y}{2E_z I_y} (2z + L) \tag{3.58}$$

where the maximum deflections appear at the middle ($z = -L/2$) and the maximum rotations appear at the ends ($z = 0$ and $z = -L$) of the cylinder.

Based on Eqs. (3.57) and (3.58), if the prescribed maximum deflections are $u_{x,\max}^0$ and $u_{y,\max}^0$, or the prescribed rotations at one end of the cylinder ($z = 0$) are $\omega_{x,0}^0$ and $\omega_{y,0}^0$, the corresponding bending moments due to these prescribed values can be obtained as:

$$M_{x,0} = 8E_z I_x u_{y,\max}^0 / L^2, \quad M_{y,0} = -8E_z I_y u_{x,\max}^0 / L^2, \tag{3.59}$$

or

$$M_{x,0} = 2E_z I_x \tan \omega_{x,0}^0 / L, \quad M_{y,0} = 2E_z I_y \tan \omega_{y,0}^0 / L. \tag{3.60}$$

It should be noted that the prescribed values $u_{x,\max}^0$, $u_{y,\max}^0$, $\omega_{x,0}^0$ and $\omega_{y,0}^0$ in Eqs. (3.59) and (3.60) include positive or negative signs which indicate the directions of deflections or rotations. The converted moments for other displacement boundary conditions can be obtained from Eq. (3.56) through a procedure similar to that above mentioned.

4 Stress analysis using the homogenization method

Having obtained the stress solutions of homogenized cylinders, the stresses in multi-layered anisotropic composite cylindrical structures can be obtained through the homogenization method. Homogenization is an approach which is used in applied mechanics to predict the macroscopic response of multi-phase or heterogeneous materials from the microscopic properties and local behaviors [25–27]. In the analysis of composite materials, homogenization is usually a process involving at least two scales, i.e., the macroscopic scale and one or more microscopic scales. The macroscopic properties and behavior are typically based on representative volume elements (RVEs) which contain the necessary microscopic information [28,29]. The homogenization based on RVEs is widely used with FEM in various fields of solid mechanics including analysis of composite

materials and structures [29]. In this paper, the proposed homogenization method for stress analysis of composite cylindrical structures is based on two scales, i.e., the cylinder and ply scales which, respectively, correspond to the macroscopic and microscopic scales. The stress analysis using the proposed homogenization method includes two aspects: (i) stresses in a layer (ply scale) are determined from the solutions of homogenized cylinders (cylinder scale) and (ii) effective material properties of the homogenized cylinders (cylinder scale) are determined from the layer material properties (ply scale) by the standard homogenization. Specifically, the proposed homogenization method for stress analysis is based on the stress solutions and the effective material properties of homogenized cylinders. The method combines the continuity condition of some stress and strain components to determine the layer stresses and strains of anisotropic composite cylindrical structures.

4.1 Stresses and strains in a layer of composite cylindrical structures

In the proposed homogenization method for stress analysis, the strains and stresses that are continuous through the thickness of a composite cylindrical structure, i.e., $\varepsilon_\theta^{(i)}$, $\varepsilon_z^{(i)}$, $\gamma_{\theta z}^{(i)}$ and $\sigma_r^{(i)}$, $\tau_{rz}^{(i)}$, $\tau_{r\theta}^{(i)}$, are taken to be equal to solutions for the homogenized cylinder under the same loading conditions, and then the remaining discontinuous stresses and strains, i.e., $\sigma_\theta^{(i)}$, $\sigma_z^{(i)}$, $\tau_{\theta z}^{(i)}$ and $\varepsilon_r^{(i)}$, $\gamma_{rz}^{(i)}$, $\gamma_{r\theta}^{(i)}$, can be obtained from the continuous strains and stresses with the layer material properties and the effective (homogenized) material properties. The basic assumptions in the homogenization method can be written as:

$$\varepsilon_\theta^{(i)} = \varepsilon_\theta, \quad \varepsilon_z^{(i)} = \varepsilon_z, \quad \gamma_{\theta z}^{(i)} = \gamma_{\theta z}, \quad \sigma_r^{(i)} = \sigma_r, \quad \tau_{rz}^{(i)} = \tau_{rz}, \quad \tau_{r\theta}^{(i)} = \tau_{r\theta}, \tag{4.1}$$

where ε_θ, ε_z, $\gamma_{\theta z}$ and σ_r, τ_{rz}, $\tau_{r\theta}$ are the strain and stress solutions for the homogenized cylinder as mentioned in Sect. 3.

From Eq. (4.1), the stress in the (i)th layer $\boldsymbol{\sigma}^{(i)}$ can be calculated through the stress $\boldsymbol{\sigma}$ of the homogenized cylinder as:

$$\boldsymbol{\sigma}^{(i)} = \boldsymbol{\Phi}^{(i)}\boldsymbol{\sigma}. \tag{4.2}$$

Equation (4.2) indicates the general relationship of stresses between the (i)th layer and the homogenized cylinder, where $\boldsymbol{\Phi}^{(i)}$ accounts for the stress discontinuity through layers and the material heterogeneity of the composite cylindrical structure. The coefficient matrix $\boldsymbol{\Phi}^{(i)}$ is determined from both the layer and the effective material properties and can be written in the following formulation:

$$\boldsymbol{\Phi}^{(i)} = \boldsymbol{D}^{*(i)}\boldsymbol{S}^{*(i)} = \begin{bmatrix} 1 & 0 & 0 & 0 & 0 & 0 \\ \Phi_{21}^{(i)} & \Phi_{22}^{(i)} & \Phi_{23}^{(i)} & \Phi_{24}^{(i)} & 0 & 0 \\ \Phi_{31}^{(i)} & \Phi_{32}^{(i)} & \Phi_{33}^{(i)} & \Phi_{34}^{(i)} & 0 & 0 \\ \Phi_{41}^{(i)} & \Phi_{42}^{(i)} & \Phi_{43}^{(i)} & \Phi_{44}^{(i)} & 0 & 0 \\ 0 & 0 & 0 & 0 & 1 & 0 \\ 0 & 0 & 0 & 0 & 0 & 1 \end{bmatrix}, \tag{4.3}$$

where

$$\boldsymbol{D}^{*(i)} = \begin{bmatrix} s_{11}^{(i)} & 0 & 0 & 0 & 0 & 0 \\ 0 & s_{22}^{(i)} & s_{23}^{(i)} & s_{24}^{(i)} & 0 & 0 \\ 0 & s_{23}^{(i)} & s_{33}^{(i)} & s_{34}^{(i)} & 0 & 0 \\ 0 & s_{24}^{(i)} & s_{34}^{(i)} & s_{44}^{(i)} & 0 & 0 \\ 0 & 0 & 0 & 0 & s_{55}^{(i)} & 0 \\ 0 & 0 & 0 & 0 & 0 & s_{66}^{(i)} \end{bmatrix}^{-1}, \tag{4.4}$$

$$\boldsymbol{S}^{*(i)} = \begin{bmatrix} s_{11}^{(i)} & 0 & 0 & 0 & 0 & 0 \\ s_{12} - s_{12}^{(i)} & s_{22} & s_{23} & s_{24} & 0 & 0 \\ s_{13} - s_{13}^{(i)} & s_{23} & s_{33} & s_{34} & 0 & 0 \\ s_{14} - s_{14}^{(i)} & s_{24} & s_{34} & s_{44} & 0 & 0 \\ 0 & 0 & 0 & 0 & s_{55}^{(i)} & 0 \\ 0 & 0 & 0 & 0 & 0 & s_{66}^{(i)} \end{bmatrix}, \tag{4.5}$$

and $s_{jl}(j, l = 1, 2, 3, 4, 5, 6)$ are the effective material compliance components of the homogenized cylinder.

After the stress $\boldsymbol{\sigma}^{(i)}$ is obtained, the strain in the layer, $\boldsymbol{\varepsilon}^{(i)}$, can be calculated from Eq. (2.3) as:

$$\boldsymbol{\varepsilon}^{(i)} = \boldsymbol{S}^{(i)}\boldsymbol{\sigma}^{(i)} = \boldsymbol{S}^{(i)}\boldsymbol{\Phi}^{(i)}\boldsymbol{\sigma}. \tag{4.6}$$

It can be seen that the stresses and strains in Eqs. (4.2) and (4.6) will converge to the homogenized solutions if the composite cylindrical structure is a homogenous cylinder with $\boldsymbol{S}^{(i)} = \boldsymbol{S}$ and $\boldsymbol{\Phi}^{(i)} = \mathbf{I}$ (unit matrix). In Eqs. (4.2)–(4.6), it may be noted that either the layer materials or the effective materials can be monoclinic anisotropic. The effective material properties of the homogenized cylinder, $s_{jl}(j, l = 1, 2, 3, 4, 5, 6)$, will be further discussed in Sect. 4.2. For the (i)th layer of the composite cylindrical structures, if the material is orthotropic with a fiber angle $\varphi^{(i)}$, the off-axial anisotropic material compliance components $s_{jl}^{(i)}(j, l = 1, 2, 3, 4, 5, 6)$, or the material compliance matrix $\boldsymbol{S}^{(i)}$, can be determined from the ply properties with the rotation angle $\varphi^{(i)}$ about the r direction. The transformation between the ply and the cylinder can be written as:

$$\boldsymbol{S}^{(i)} = \left(\boldsymbol{T}_{\varphi}^{(i)}\right)^{\mathrm{T}} \boldsymbol{S}_0^{(i)} \boldsymbol{T}_{\varphi}^{(i)} \tag{4.7}$$

where $\boldsymbol{S}_0^{(i)}$ is the material compliance matrix in the material directions of the (i)th layer; $\boldsymbol{T}_{\varphi}^{(i)}$ is the transformation matrix, and

$$\boldsymbol{S}_0^{(i)} = \begin{bmatrix} 1/E_3^{(i)} & -\nu_{23}^{(i)}/E_2^{(i)} & -\nu_{13}^{(i)}/E_1^{(i)} & 0 & 0 & 0 \\ -\nu_{32}^{(i)}/E_3^{(i)} & 1/E_2^{(i)} & -\nu_{12}^{(i)}/E_1^{(i)} & 0 & 0 & 0 \\ -\nu_{31}^{(i)}/E_3^{(i)} & -\nu_{21}^{(i)}/E_2^{(i)} & 1/E_1^{(i)} & 0 & 0 & 0 \\ 0 & 0 & 0 & 1/G_{12}^{(i)} & 0 & 0 \\ 0 & 0 & 0 & 0 & 1/G_{13}^{(i)} & 0 \\ 0 & 0 & 0 & 0 & 0 & 1/G_{23}^{(i)} \end{bmatrix}, \tag{4.8}$$

$$\boldsymbol{T}_{\varphi}^{(i)} = \begin{bmatrix} 1 & 0 & 0 & 0 & 0 & 0 \\ 0 & \cos^2\varphi^{(i)} & \sin^2\varphi^{(i)} & -\sin 2\varphi^{(i)} & 0 & 0 \\ 0 & \sin^2\varphi^{(i)} & \cos^2\varphi^{(i)} & \sin 2\varphi^{(i)} & 0 & 0 \\ 0 & \frac{1}{2}\sin 2\varphi^{(i)} & -\frac{1}{2}\sin 2\varphi^{(i)} & \cos 2\varphi^{(i)} & 0 & 0 \\ 0 & 0 & 0 & 0 & \cos\varphi^{(i)} & \sin\varphi^{(i)} \\ 0 & 0 & 0 & 0 & -\sin\varphi^{(i)} & \cos\varphi^{(i)} \end{bmatrix} \tag{4.9}$$

where $E_1^{(i)}$, $E_2^{(i)}$, $E_3^{(i)}$, $G_{12}^{(i)}$, $G_{13}^{(i)}$, $G_{23}^{(i)}$, $\nu_{12}^{(i)}$, $\nu_{13}^{(i)}$, $\nu_{23}^{(i)}$ are nine independent engineering elastic constants of the orthotropic material in the (i)th layer.

The stress in the (i)th layer under any combination of the loads discussed in Sect. 3 can be obtained from superposing the stress in a corresponding loading condition, i.e.,:

$$\boldsymbol{\sigma}_{\mathrm{com}}^{(i)} = \sum_{j=1}^{N_F} \boldsymbol{\sigma}_{F_j}^{(i)} = \boldsymbol{\Phi}^{(i)} \sum_{j=1}^{N_F} \boldsymbol{\sigma}_{F_j} \tag{4.10}$$

where $\boldsymbol{\sigma}_{\text{com}}^{(i)}$ and $\boldsymbol{\sigma}_{F_j}^{(i)}$ are stress arrays in the (i)th layer due to the combined and single loads, respectively, and $\boldsymbol{\sigma}_{F_j}$ is the stress array solution of the homogenized cylinder due to the single load; N_F is the total number of applied loads.

The stresses and strains along the material directions in the (i)th layer, $\boldsymbol{\sigma}_0^{(i)}$ and $\boldsymbol{\varepsilon}_0^{(i)}$ in the cylindrical coordinate system, can be obtained from the transformation as:

$$\boldsymbol{\sigma}_0^{(i)} = \boldsymbol{T}_{\varphi}^{(i)} \boldsymbol{\sigma}^{(i)}, \quad \boldsymbol{\varepsilon}_0^{(i)} = \left(\boldsymbol{T}_{\varphi}^{(i)}\right)^{-\mathrm{T}} \boldsymbol{\varepsilon}^{(i)}. \tag{4.11}$$

4.2 Effective material properties of composite cylindrical structures

Effective material properties of laminated structures provide an efficient way to study the overall behavior of this kind of structures. In this paper, the effective material properties are used to calculate the stress solutions of homogenized cylinders, and then these solutions are used in Eqs. (4.2) and (4.6) to determine the layer stresses and strains of composite cylindrical structures. Several researches have been presented for studies on the effective material properties of composite laminates in literature [30–33]. The authors [34] have proposed a force-displacement equivalence method to determine the effective elastic constants of globally orthotropic composite cylindrical structures, where the non-constant stresses and strains in each layer are considered. This method, however, is not suitable for general anisotropic composite cylindrical structures because more elastic constants are coupled together into the equivalent equations. The comparison showed that for thin-walled or moderately thick-walled structures, the effective elastic constants from the force-displacement equivalence method are similar to those from lamination theories based on linear layer stresses and strains. This implies that the effective material properties from the lamination theories can be used for thin-walled or moderately thick-walled composite cylindrical structures. Pagano [31] presented a general formulation of the effective elastic constants for a laminated body with general anisotropic materials. For multi-layered composite cylindrical structures, the effective elastic constants can be rewritten from Pagano's formulation as:

$$\begin{cases} d_{jl} = \sum_{i=1}^{n} V^{(i)} d_{jl}^{(i)} + d_{11} \left(\sum_{i=1}^{n} \frac{V^{(i)} d_{1j}^{(i)}}{d_{11}^{(i)}} \right) \left(\sum_{i=1}^{n} \frac{V^{(i)} d_{1l}^{(i)}}{d_{11}^{(i)}} \right) - \sum_{i=1}^{n} \frac{V^{(i)} d_{1j}^{(i)} d_{1l}^{(i)}}{d_{11}^{(i)}}, \\ d_{11} = \left(\sum_{i=1}^{n} \frac{V^{(i)}}{d_{11}^{(i)}} \right)^{-1}, \quad d_{j'l'} = \frac{1}{\Delta} \sum_{i=1}^{n} \frac{V^{(i)} d_{j'l'}^{(i)}}{\Delta^{(i)}}, \quad d_{jl'} = d_{l'j} = 0, \end{cases} \tag{4.12}$$

where $j = 1, 2, 3, 4$, $l = 2, 3, 4$ and $j', l' = 5, 6$ with $d_{lj} = d_{jl}$, and

$$\begin{cases} \Delta^{(i)} = d_{55}^{(i)} d_{66}^{(i)} - d_{56}^{(i)} d_{56}^{(i)}, \\ \Delta = \left(\sum_{i=1}^{n} V^{(i)} d_{55}^{(i)} / \Delta^{(i)} \right) \left(\sum_{i=1}^{n} V^{(i)} d_{66}^{(i)} / \Delta^{(i)} \right) - \left(\sum_{i=1}^{n} V^{(i)} d_{56}^{(i)} / \Delta^{(i)} \right)^2, \end{cases} \tag{4.13}$$

$$V^{(i)} = \frac{r_{i+1}^2 - r_i^2}{b^2 - a^2} = \frac{c_{i+1}^2 - c_i^2}{1 - c^2}. \tag{4.14}$$

It should be noted that the integrals in Pagano's original formulation are replaced by finite summations in Eq. (4.12). The volume fraction of a layer in Eq. (4.14) is based on cross section area instead of thickness as that in normal lamination theories [32,33]. This formulation of the volume fraction can account for the effect of stacking sequence of multi-layered composite cylindrical structures. After the effective material stiffness components are determined from Eq. (4.12), the effective material compliance components can be determined from Eq. (2.7) with the relationship $\boldsymbol{S} = \boldsymbol{D}^{-1}$.

4.3 Effective stiffness coefficients of composite cylindrical structures

Now we consider several important strain components which indicate the overall deformation characteristics of the composite cylindrical structures. Under the loading conditions as shown in Fig. 2a, the axial strain $\varepsilon_z^{(i)}$ and shear strain $\gamma_{\theta z}^{(i)}$ in the (i)th layer can be obtained from Eqs. (4.1) and (4.6) as the following concise formulations:

$$\left(\varepsilon_z^{(i)}\right)_{(a)} = (\varepsilon_z)_{(a)} = C/E_z, \quad \left(\gamma_{\theta z}^{(i)}\right)_{(a)} = (\gamma_{\theta z})_{(a)} = \Upsilon \rho, \tag{4.15}$$

where $E_z = 1/s_{33}$ and the subscript "(a)" denotes the strain values under the loading conditions as shown in Fig. 2a.

It can be seen that the axial strain is constant and the shear strain is linear on the cross section of the composite cylindrical structures due to the loads as shown in Fig. 2a. We define $\varepsilon_0 = (\varepsilon_z)_{(a)}$ and $\gamma_0 = (\gamma_{\theta z})_{(a)}/r$. They denote constant axial deformation and constant hoop rotation per length of the composite cylindrical structures, respectively. With the aid of Eqs. (3.11) and (4.15), ε_0 and γ_0 can be written as:

$$\varepsilon_0 = \frac{\Sigma_2 P}{2\pi b^2 \Sigma_0 E_z} - \frac{\Sigma_1 M_t}{2\pi b^3 \Sigma_0 E_z} + \frac{C_p}{E_z}, \quad \gamma_0 = \frac{B_1 M_t}{2\pi b^4 \Sigma_0} - \frac{B_2 P}{2\pi b^3 \Sigma_0} + \frac{\Upsilon_p}{b}. \tag{4.16}$$

For the loading conditions with bending moments as shown in Fig. 2c, the constant curvature χ_0 due to the bending moments can be expressed as:

$$\chi_0 = \frac{M_b}{E_z I} \tag{4.17}$$

where $M_b = \sqrt{M_x^2 + M_y^2}$.

It may be noted that for anisotropic composite cylindrical structures the extensional and torsional deformations are coupled with each other, but they are uncoupled with the curvature. Then the axial force P, twisting moment M_t and bending moment M_b can be rewritten with Eqs. (4.16) and (4.17) as:

$$\begin{bmatrix} P \\ M_t \\ M_b \end{bmatrix} = \begin{bmatrix} E_z A & D_{12} & 0 \\ D_{21} & G_{\theta z} J & 0 \\ 0 & 0 & E_z I \end{bmatrix} \begin{bmatrix} \varepsilon_0 - \varepsilon_0^p \\ \gamma_0 - \gamma_0^p \\ \chi_0 \end{bmatrix} \tag{4.18}$$

where $G_{\theta z} = 1/s_{44}$; ε_0^p and γ_0^p are the constant axial deformation and hoop rotation per length due to internal pressure p and/or external pressure q only (i.e., $\varepsilon_0^p = \gamma_0^p = 0$ if $p = q = 0$), and

$$\varepsilon_0^p = C_p/E_z, \quad \gamma_0^p = \Upsilon_p/b, \tag{4.19}$$

$$D_{12} = 2\pi b^3 \Sigma_1, \quad D_{21} = 2\pi b^3 B_2 E_z. \tag{4.20}$$

The parameters $E_z A$, $G_{\theta z} J$, $E_z I$ and D_{12} (or D_{21}) in Eq. (4.18) are, respectively, defined as the effective axial, torsional, bending and coupling stiffness coefficients of the composite cylindrical structures, which indicate the overall performance of resisting deformations of the composite cylindrical structures. The parameters A, J and I denote the effective cross sectional area, area moment of inertia and area polar moment of inertia, respectively, and

$$A = A_0 + A^*, \quad J = J_0 + J^*, \quad I = I_0 + I^*, \tag{4.21}$$

$$A_0 = \pi b^2 \left(1 - c^2\right), \quad J_0 = \pi b^4 \left(1 - c^4\right)/2, \quad I_0 = \pi b^4 \left(1 - c^4\right)/4, \tag{4.22}$$

$$\begin{cases} A^* = \pi b^2 \left(2B_1 + c^2 - 1\right), \quad J^* = \pi b^4 \left(4\Sigma_2/G_{\theta z} + c^4 - 1\right)/2, \\ I^* = -\pi b^4 \left[\frac{\lambda^* \left(1 - c^4\right)}{4} + \sum_{j=1}^{4} H_j m_j^* K_{m_j}\right], \end{cases} \tag{4.23}$$

The constant parameters C_p, Υ_p, B_1, B_2, Σ_1, Σ_2, H_j, λ^*, m_j^* and K_{m_j} in Eqs. (4.19), (4.20) and (4.23) can be found in Eqs. (3.12)–(3.15), (3.34) and (3.37)–(3.39).

It can be verified that $D_{12} = D_{21}$ with $\Sigma_1 = B_2 E_z$. The coupling stiffness coefficient D_{12} indicates the coupling effect between axial and torsional loads, which occurs for globally anisotropic composite cylindrical structures. It should be noted that A, J and I are usually based on both geometrical and material parameters, and their formulations imply the effects of material anisotropy. Therefore, $A \neq A_0$, $J \neq J_0$ and $I \neq I_0$ for globally anisotropic composite cylindrical structures, where A_0, I_0 and $J_0 = 2I_0$ are the cross sectional area and the area moments of inertia based on geometrical parameters only. The coefficients D_{12} (or D_{21}), A^*, J^* and I^* in Eqs. (4.20) and (4.23) are due to the differences among elastic moduli, Poisson's ratios and nonzero extension-shear coupling coefficients of the anisotropic materials. It can be verified that $A = A_0$ ($A^* = 0$) and $I = I_0$ ($I^* = 0$) for globally isotropic composite cylindrical structures only; $J = J_0$($J^* = 0$) and $D_{12} = D_{21} = 0$ for globally isotropic or orthotropic composite cylindrical structures.

With Eqs. (3.56)–(3.58), the bending stiffness coefficient $E_z I$ can also be used to calculate rotations or deflections off-axial direction of long composite cylindrical structures due to bending moments. If the composite cylindrical structures are globally orthotropic, the expressions of A and I in Eq. (4.21) are reduced to:

$$A = A_0 - 2\pi b^2 \delta_1 \left\{ \frac{1-c^2}{2} \cdot \frac{s_{13}+s_{23}}{s_{33}} - \sum_{j=1}^{2} \left[\frac{\left(1-c^{k_j+1}\right)^2}{1-c^{2k_j}} \cdot \frac{s_{13}+k_j s_{23}}{\left(k_j+1\right) s_{33}} \right] \right\}, \tag{4.24}$$

$$I = I_0 - \pi b^4 \lambda_1 \left\{ \frac{1-c^4}{4} \cdot \frac{s_{13}+3s_{23}}{s_{33}} - \sum_{j=1}^{2} \left[\frac{\left(1-c^{m_j+2}\right)^2}{1-c^{2m_j}} \cdot \frac{s_{13}+\left(m_j+1\right) s_{23}}{\left(m_j+2\right) s_{33}} \right] \right\} \tag{4.25}$$

where k_j, δ_1, m_j and λ_1 are defined in Eqs. (3.23), (3.24), (3.40) and (3.41), respectively.

These two formulations were also presented by Lekhnitskii [1] in his equations (43.4) and (43.18), respectively, for homogenous hollow orthotropic cylinders. It should be noted that the coefficient $1-c^{2k_j}$ in Eq. (4.24) is omitted in Lekhnitskii's equation (43.4), and the minus sign $(-)$ before $2\pi b^2$ in Eq. (4.24) is also mistaken for a plus sign (+) in Lekhnitskii's equation (43.4).

5 Examples and results

5.1 Effective stiffness coefficients of anisotropic cylinders

This example shows several anisotropy parameters changing with different anisotropic materials. Hollow cylinders made of fiber-reinforced composite materials with different fiber angles are used in the example. The material will present monoclinic anisotropy in the cylindrical coordinate system. For simplicity, the cylinder has one layer with a composite material. The inner and outer radii of the cylinder are $a = 140$ and $b = 150$mm, respectively. Two typical composite systems, i.e., carbon/epoxy (T300/LY5052) [16] and glass/epoxy (E-glass/LY556) [35], are considered in the analysis. The material properties are listed in Table 1.

Figure 3 shows the extension-shear coupling coefficients of the composite cylinder with different fiber angles in the cylindrical coordinate system. It can be seen that the two coefficients on the $\theta - z$ surface ($\eta_{\theta,\theta z}$ and $\eta_{z,\theta z}$) may have significant values and the two through-thickness coefficients ($\eta_{r,\theta z}$ and $\xi_{rz,r\theta}$) have less significant values. Figure 4 shows the effective axial, torsional, bending and coupling stiffness coefficients of the composite cylinder with different fiber angles, where the values are normalized by those based on the cross sectional area (A_0) or area moments of inertia (I_0 and J_0). It can be seen that the normalized axial, torsional and coupling stiffness coefficients change significantly with some fiber angles, whereas the normalized bending stiffness coefficient hardly changes with all fiber angles. This indicates that the material anisotropy has little effect on the bending stiffness coefficient but significant effect on other stiffness coefficients. This is because the axial and torsional loads are generally coupled for anisotropic materials, but they are uncoupled from bending moments. Therefore, the bending stiffness coefficient may be estimated with I_0 in Eq. (4.22) instead of I in Eq. (4.21), but other stiffness coefficients need to be calculated with A or J in Eq. (4.21) for the fiber-reinforced composite materials. These coefficients have a similar changing trend with fiber angles for carbon/epoxy and glass/epoxy, but the material anisotropy of the carbon/epoxy shows a more significant effect on the coefficients. The reason may be that the differences among elastic moduli of the carbon/epoxy are much larger than those of the glass/epoxy.

Table 1 Material properties of two composite systems

Engineering constants	Carbon/epoxy (T300/LY5052) [16]	Glass/epoxy (E-glass/LY556) [35]
E_1 (GPa)	135.0	53.48
$E_2 = E_3$ (GPa)	8.0	17.7
$G_{12} = G_{13}$ (GPa)	3.8	5.83
G_{23} (GPa)	2.7	6.32
$v_{12} = v_{13}$	0.27	0.278
v_{23}	0.49	0.40

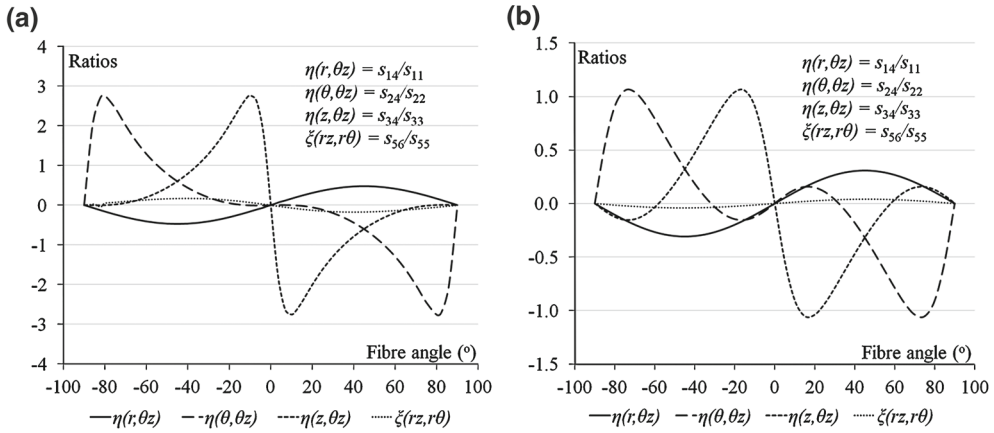

Fig. 3 Extension-shear coupling coefficients of the cylinder with **a** carbon/epoxy and **b** glass/epoxy of different fiber angles

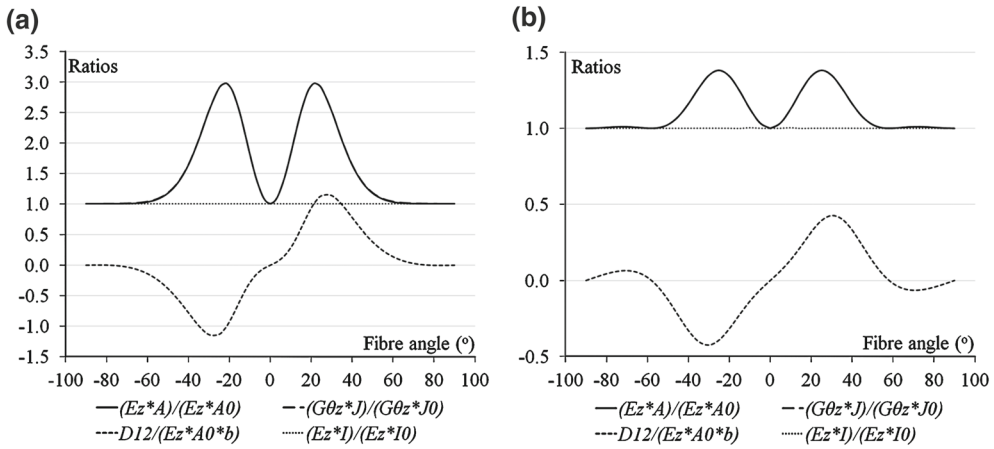

Fig. 4 Effective stiffness coefficients of the cylinder with **a** carbon/epoxy and **b** glass/epoxy of different fiber angles

It may be noted that the normalized axial and torsional stiffness coefficients are quite similar (nearly overlapped curves) in Fig. 4. The value of D_{12} may be negative depending on the fiber angles, as shown Fig. 4a, b. A negative value of D_{12} means that the axial and shear deformations due to the axial force or torsion are both positive or both negative. For any two opposite fiber angles (e.g., $\pm 30°$), all the extension-shear coupling coefficients and D_{12} have opposite values, whereas the effective axial, torsional and bending stiffness coefficients have the same values.

5.2 Stress analysis of a composite riser

In this example, a 22-layer composite riser used in offshore oil production is analyzed to demonstrate the application of the present stress analysis method. The composite riser consists of a liner (Titanium), twenty composite layers (carbon/epoxy) and an outer layer (polymer) [36]. The stacking sequence of the composite layers is $[45/-45/15/80]_5$ (from inner to outer layers). The composite material is T300/LY5052, and the properties are listed in Table 1. The material properties of the liner (Titanium) are $E = 120\,\text{GPa}$ and $\upsilon = 0.33$. The material properties of the outer layer (polymer) are $E = 3.0\,\text{GPa}$ and $\upsilon = 0.40$. The geometrical properties of the riser components are listed in Table 2, where the thickness of the 80° ply is 1.143 mm and the thickness of each ply with other angles is 0.508 mm.

The effective material stiffness matrix of the homogenized composite riser can be calculated from Eq. (4.12) as:

Table 2 Geometry parameters of the composite riser [36]

Parameters	Values
Length L (m)	10
Inner radius, a (mm)	140.00
Outer radius, b (mm)	160.335
Liner thickness (mm)	5.0
Composite layers ($[45/-45/15/80]_5$) thickness (mm)	13.335
Outer layer thickness (mm)	2.0

$$\boldsymbol{D} = \begin{bmatrix} 12.55 & 5.951 & 6.141 & -0.096 & 0 & 0 \\ 5.951 & 82.50 & 24.65 & 6.213 & 0 & 0 \\ 6.141 & 24.65 & 62.43 & 3.911 & 0 & 0 \\ -0.096 & 6.213 & 3.911 & 22.95 & 0 & 0 \\ 0 & 0 & 0 & 0 & 3.110 & 0.089 \\ 0 & 0 & 0 & 0 & 0.089 & 3.288 \end{bmatrix} \text{GPa}, \tag{5.1}$$

and the effective elastic constants of the composite riser (e.g., E_θ, E_z, $G_{\theta z}$, etc.) can be obtained from the effective material compliances with the relationship $\boldsymbol{S} = \boldsymbol{D}^{-1}$.

Six loading conditions are considered in the analysis: (1) internal pressure $p = 1.5$ MPa and external pressure $q = 1$ MPa, (2) axial force $P = 1$ kN, (3) torsion $M_t = 1$ kN m, (4) axial shear $\tau_{z,0} = 1$MPa, (5) in-plane shear $\tau_{\theta,0} = 1$ MPa and (6) bending moment $M_x = 1$ kN m. The axial and in-plane shears are acting on the external surface of the composite riser. Under these loading conditions, the analysis results from the present method are compared with the numerical solutions from FEM. Two FE models, namely FEM(A) and FEM(B), are considered in the analysis. The model FEM(A) is based on multiple solid elements through the thickness, i.e., each layer is modeled with one through-thickness element and there are in total, 22 elements through the thickness. The model FEM(B) is based on composite elements through the thickness, i.e., the liner and the outer layer are modeled with one through-thickness element, respectively, and the 20 composite layers are modeled with only one through-thickness element. Linear brick solid elements with reduced integration scheme (C3D8R) are used in both FE models [23]. This element type is a three-dimensional 8-node hexahedral element that has totally 24 displacement degrees of freedom (DOFs), with 3 DOFs at one node. In the model FEM(B), there are only three through-thickness elements which represent the titanium liner, the 20 composite layers and the outer polymer layer, respectively. In the elements representing the composite layers, 20 section points are allocated through the element thickness with assigned corresponding material orientations (45°, −45°, 15°, 80°) to model the composite layers with different fiber angles.

The effective axial, torsional, bending and coupling stiffness coefficients of the composite riser are calculated from Eqs. (4.20) and (4.21) with E_z and $G_{\theta z}$. The results are also compared with numerical values from the both FE models, as shown in Table 3. The results from FEM are obtained from the back-calculation with the numerical axial and shear strains under three uniaxial loading conditions (i.e., axial extension, torsion and bending) through the following equations:

$$\begin{cases} E_z A = P \cdot (\gamma_0)_{M_t} / \left[(\varepsilon_0)_P (\gamma_0)_{M_t} - (\varepsilon_0)_{M_t} (\gamma_0)_P \right], \\ G_{\theta z} J = M_t \cdot (\varepsilon_0)_P / \left[(\varepsilon_0)_P (\gamma_0)_{M_t} - (\varepsilon_0)_{M_t} (\gamma_0)_P \right], \\ D_{12} = -E_z A \cdot (\varepsilon_0)_{M_t} / (\gamma_0)_{M_t}, \\ D_{21} = -G_{\theta z} J \cdot (\gamma_0)_P / (\varepsilon_0)_P, \\ E_z I = M_x b / (\varepsilon_z)_{M_x} \big|_{r=b} \end{cases} \tag{5.2}$$

where the subscripts "P", "M_t" and "M_x" denote the strain values under the corresponding uniaxial loading conditions.

Figures 5, 6, 7, 8, 9, 10, 11 and 12 show the stresses and strains in each layer through the thickness of the composite riser under different loading conditions. Under axial and in-plane shear loading conditions, it may be noted that the stresses and strains predicted from the present method in Figs. 7 and 8 based on Eq. (3.22) are exact solutions for composite cylindrical structures. Generally, the two FE models predict very similar results of

Table 3 Effective stiffness coefficients of the composite riser

Coefficients	Present method	FEM(A)	FEM(B)	Difference from FEM	
				FEM(A) (%)	FEM(B) (%)
E_zA (N)	1.026E+09	1.013E+09	1.013E+09	1.28	1.28
$G_{\theta z}J$ (N mm^2)	9.765E+12	9.310E+12	9.303E+12	4.89	4.97
D_{12} (N mm)	6.486E+09	6.565E+09	6.520E+09	−1.20	−0.52
D_{21} (N mm)	6.486E+09	6.508E+09	6.558E+09	−0.34	−1.10
E_zI (N mm^2)	1.158E+13	1.093E+13	1.091E+13	5.95	6.14

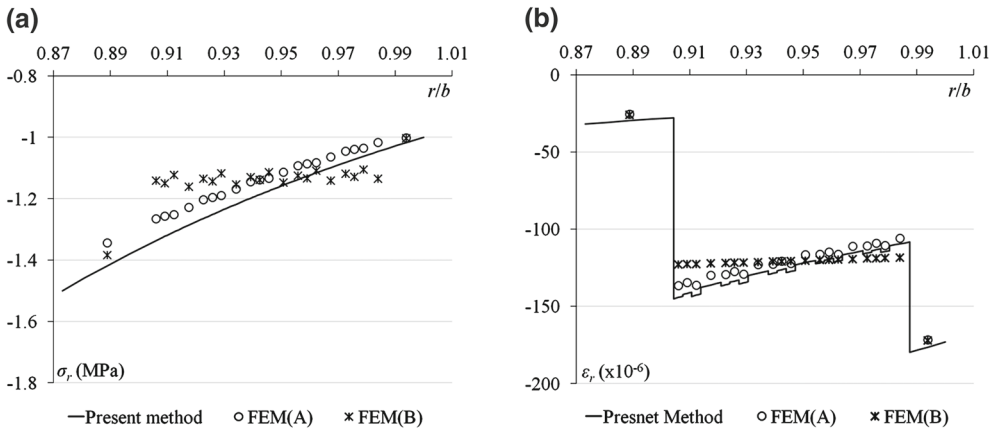

Fig. 5 Distribution of **a** radial stresses and **b** radial strains under internal and external pressures

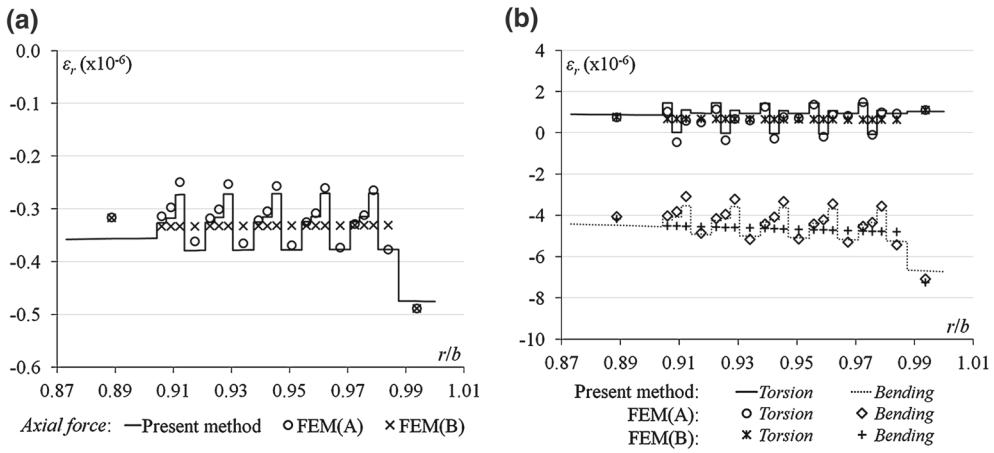

Fig. 6 Distribution of radial strains **a** under axial force and **b** under torsion and bending moment

stresses and strains on the cylindrical surface ($\theta - z$ surface), but different results of stresses and strains through the thickness (r direction), as shown in Figs. 5, 6, 7 and 8. The through-thickness strains $\varepsilon_r^{(i)}$, $\gamma_{rz}^{(i)}$ and $\gamma_{r\theta}^{(i)}$ in the composite layers predicted from FEM(B) are nearly linear due to the strain compatibility assumptions in this model, and therefore, the through-thickness strains as well as stresses $\sigma_r^{(i)}$, $\tau_{rz}^{(i)}$ and $\tau_{r\theta}^{(i)}$ are not correctly predicted from this model. The values of radial stresses under the axial force, torsion and bending moment are very small (nearly zero) compared with other stress components, and so they are neglected in the comparison. FEM(A) predicts more reasonable through-thickness stresses and strains than FEM(B), and it can be seen that the results from the present method agree reasonably with those from FEM(A). Since the results of stresses and strains on $\theta - z$ surface are very similar for both FE models, the results from the present method are compared only with those from FEM(B) for simplicity, as shown in Figs. 9, 10, 11 and 12. The results show that the stresses on $\theta - z$ surface ($\sigma_\theta^{(i)}$, $\sigma_z^{(i)}$ and $\tau_{\theta z}^{(i)}$) are significantly discontinuous, but the corresponding

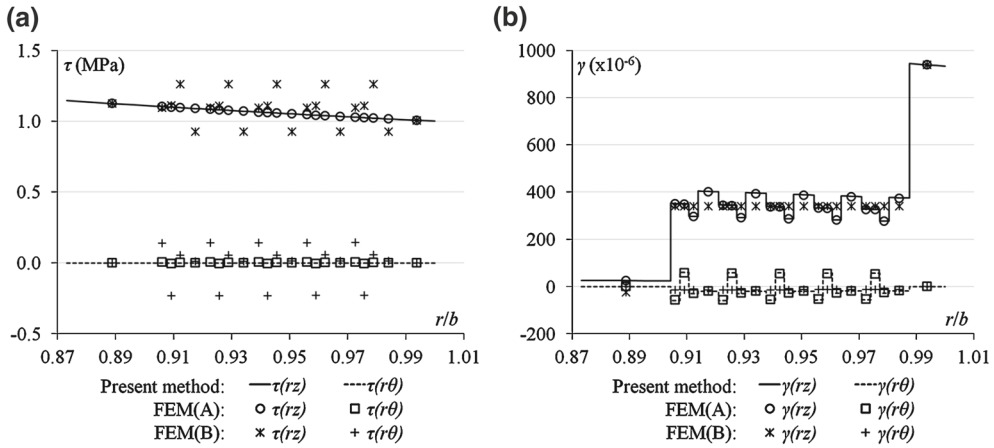

Fig. 7 Distribution of **a** stresses and **b** strains under axial shear

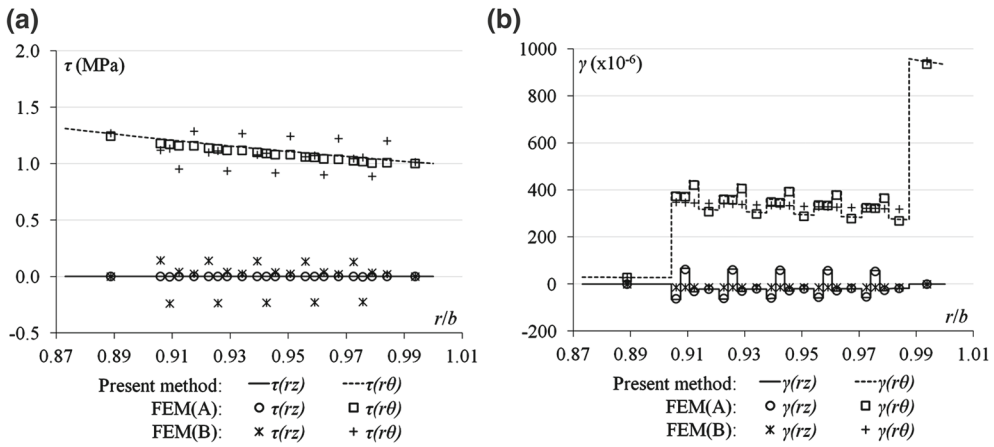

Fig. 8 Distribution of **a** stresses and **b** strains under in-plane shear

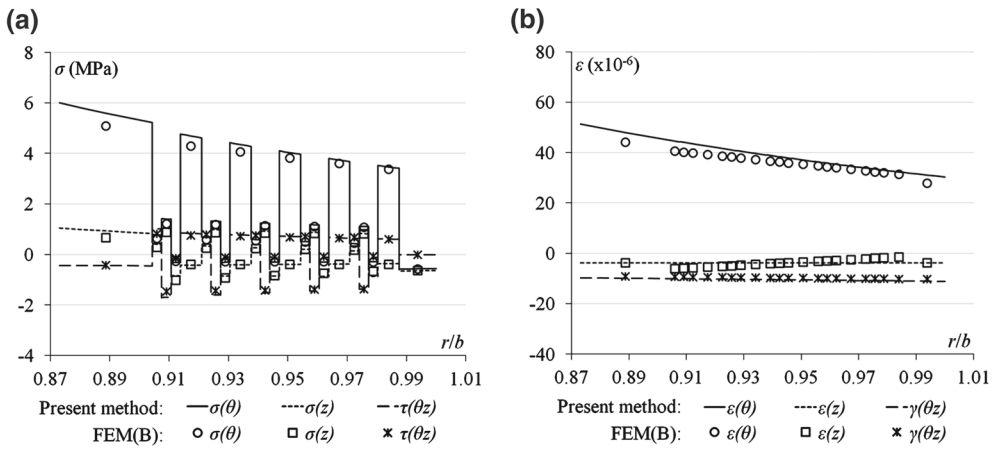

Fig. 9 Distribution of **a** stresses and **b** strains under internal and external pressures

strains ($\varepsilon_\theta^{(i)}$, $\varepsilon_z^{(i)}$ and $\gamma_{\theta z}^{(i)}$) are continuous through different layers of the composite riser. This is reverse for the stresses and strains through the thickness, where the stresses $\sigma_r^{(i)}$, $\tau_{rz}^{(i)}$ and $\tau_{r\theta}^{(i)}$ are continuous but the strains $\varepsilon_r^{(i)}$, $\gamma_{rz}^{(i)}$ and $\gamma_{r\theta}^{(i)}$ are discontinuous through different layers, as shown in Figs. 5, 6, 7 and 8. The radial strains

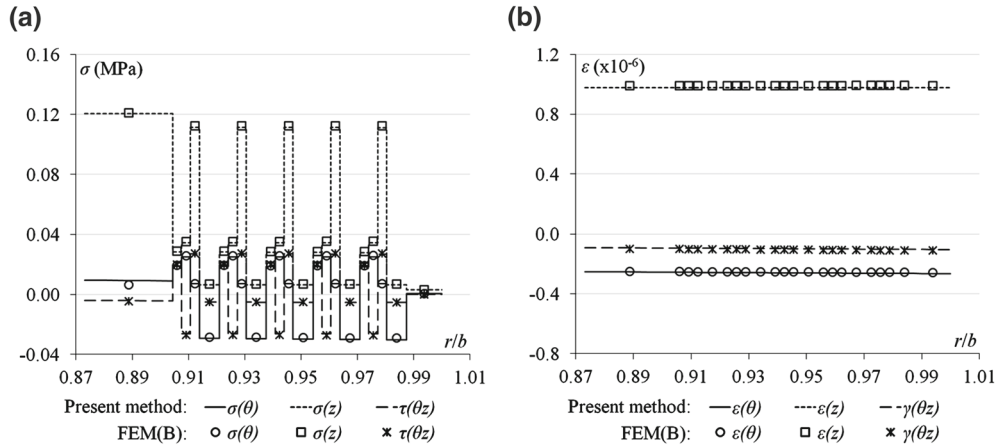

Fig. 10 Distribution of **a** stresses and **b** strains under axial force

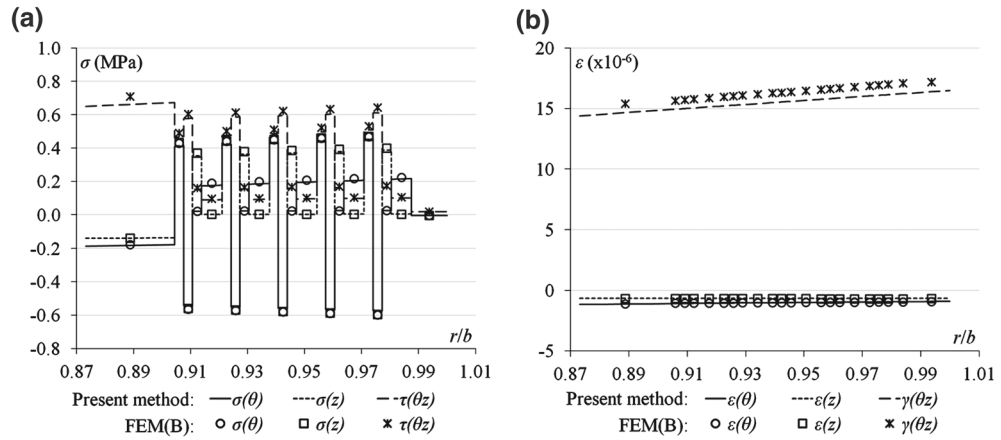

Fig. 11 Distribution of **a** stresses and **b** strains under torsion

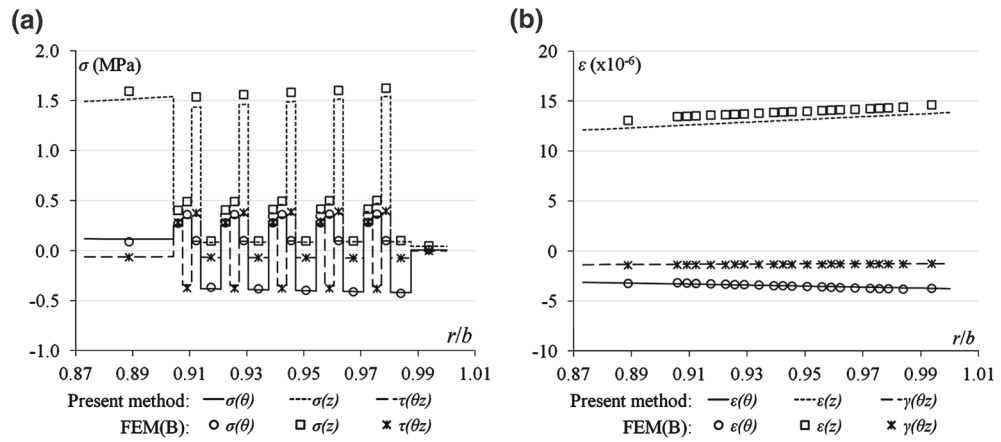

Fig. 12 Distribution of **a** stresses and **b** strains under bending moment

are dominated under internal and external pressures, but they are insignificant under axial force or torsion. The comparison demonstrates that the present method can reasonably and efficiently predict the stresses and strains both on the cylindrical surface and through the thickness of multi-layered composite cylindrical structures.

6 Conclusions

This paper presents a general and efficient stress analysis strategy for multi-layered hollow composite cylindrical structures with anisotropic materials. The stress solutions of homogenized hollow anisotropic cylinders under pressure, axial force, torsion, shears and bending moments are presented with explicit formulations based on both force-type and displacement-type boundary conditions. All the parameters required in the solutions are consistently derived from corresponding boundary conditions. The stresses and strains in each layer are determined from the solutions of homogenized hollow anisotropic cylinders, effective material properties of the composite cylindrical structures and material properties of the layer. The effective axial, torsional, bending and coupling stiffness coefficients of multi-layered hollow composite cylindrical structures are also determined from the continuous strains solutions. These coefficients indicate the overall performance of resisting deformation of the composite cylindrical structures, which can be useful in global analysis of long pipe systems. The proposed stress analysis method is applicable to thin-walled or moderately thick-walled hollow cylindrical structures with various layers of general monoclinic anisotropic materials, typically for the hollow composite cylindrical structures with many layers of arbitrary balanced or unbalanced filament-winding angles.

The examples showed that the material anisotropy may have significant effects on the effective axial, torsional and coupling stiffness coefficients of composite cylindrical structures. This means that the material anisotropy must be considered in calculating these stiffness coefficients because the axial and torsional loads are generally coupled for anisotropic materials. On the other hand, the material anisotropy may have insignificant effects on the effective bending stiffness coefficient because the bending moments are uncoupled with other loads. Stresses and strains in each layer of a 22-layer composite offshore production riser subjected to internal and external pressures, axial force, torsion, shears and bending moment were analyzed using the present method. The results are compared with the numerical solutions from FEM, and a reasonably good agreement is observed. The validity and efficiency of the present method are demonstrated through the example. This method provides an efficient and easy-to-use tool for stress analysis of composite cylindrical structures, such as tubes, pipes, risers, etc. It can be potentially used in failure and fatigue analyses of these composite cylindrical structures.

Acknowledgments The authors gratefully acknowledge the support from Singapore A*STAR (Agency for Science, Technology and Research) through the Project No. 1123004033 for MIMO (Materials Innovation for Marine and Offshore Applications).

Appendix: The differential operators in the cylindrical coordinate system

$$\boldsymbol{\nabla}_1 = \begin{bmatrix} \frac{\partial}{\partial r}+\frac{1}{r} & -\frac{1}{r} & 0 & 0 & \frac{\partial}{\partial z} & \frac{\partial}{r\partial\theta} \\ 0 & \frac{\partial}{r\partial\theta} & 0 & \frac{\partial}{\partial z} & 0 & \frac{\partial}{\partial r}+\frac{2}{r} \\ 0 & 0 & \frac{\partial}{\partial z} & \frac{\partial}{r\partial\theta} & \frac{\partial}{\partial r}+\frac{1}{r} & 0 \end{bmatrix}, \tag{A.1}$$

$$\boldsymbol{\nabla}_1' = \begin{bmatrix} \frac{\partial}{\partial r} & \frac{1}{r} & 0 & 0 & \frac{\partial}{\partial z} & \frac{\partial}{r\partial\theta} \\ 0 & \frac{\partial}{r\partial\theta} & 0 & \frac{\partial}{\partial z} & 0 & \frac{\partial}{\partial r}-\frac{1}{r} \\ 0 & 0 & \frac{\partial}{\partial z} & \frac{\partial}{r\partial\theta} & \frac{\partial}{\partial r} & 0 \end{bmatrix}^{\mathrm{T}}, \tag{A.2}$$

$$\begin{cases} L_2'^{(i)} = \beta_{44}^{(i)}\frac{\partial^2}{\partial r^2}+\beta_{55}^{(i)}\frac{\partial^2}{r^2\partial\theta^2}+\beta_{44}^{(i)}\frac{\partial}{r\partial r}, \\ L_3'^{(i)} = -\beta_{24}^{(i)}\frac{\partial^3}{\partial r^3}-\left(\beta_{14}^{(i)}+\beta_{56}^{(i)}\right)\frac{\partial^3}{r^2\partial r\partial\theta^2}-\left(\beta_{14}^{(i)}-2\beta_{24}^{(i)}\right)\frac{\partial^2}{r\partial r^2}, \\ L_3''^{(i)} = L_3'^{(i)}-3\beta_{24}^{(i)}\frac{\partial^2}{r\partial r^2}+\left(\beta_{14}^{(i)}+\beta_{56}^{(i)}\right)\frac{\partial^2}{r^3\partial\theta^2}, \\ L_4'^{(i)} = \beta_{22}^{(i)}\frac{\partial^4}{\partial r^4}+\left(2\beta_{12}^{(i)}+\beta_{66}^{(i)}\right)\frac{\partial^4}{r^2\partial r^2\partial\theta^2}+\beta_{11}^{(i)}\frac{\partial^4}{r^4\partial\theta^4} \\ \qquad +2\beta_{22}^{(i)}\frac{\partial^3}{r\partial r^3}-\left(2\beta_{12}^{(i)}+\beta_{66}^{(i)}\right)\frac{\partial^3}{r^3\partial r\partial\theta^2} \\ \qquad -\beta_{11}^{(i)}\frac{\partial^2}{r^2\partial r^2}+\left(2\beta_{11}^{(i)}+2\beta_{12}^{(i)}+\beta_{66}^{(i)}\right)\frac{\partial^2}{r^4\partial\theta^2}+\beta_{11}^{(i)}\frac{\partial}{r^3\partial r}. \end{cases} \tag{A.3}$$

References

1. Lekhnitskii, S.G.: Theory of Elasticity of an Anisotropic Body. Mir Publishers, Moscow (1981)
2. Jolicoeur, C., Cardou, A.: Analytical solution for bending of coaxial orthotropic cylinders. J. Eng. Mech. ASCE **120**, 2556–2574 (1994)
3. Chouchaoui, C.S., Ochoa, O.O.: Similitude study for a laminated cylindrical tube under tensile, torsion, bending, internal and external pressure. Part I: governing equations. Compos. Struct. **44**, 221–229 (1999)
4. Chouchaoui, C.S., Parks, P., Ochoa, O.O.: Similitude study for a laminated cylindrical tube under tensile, torsion, bending, internal and external pressure. Part II: scale models. Compos. Struct. **44**, 231–236 (1999)
5. Wild, P.M., Vickers, G.W.: Analysis of filament-wound cylindrical shells under combined centrifugal, pressure and axial loading. Compos. Part A Appl. S. **28**, 47–55 (1997)
6. Parnas, L., Katirci, N.: Design of fiber-reinforced composite pressure vessels under various loading conditions. Compos. Struct. **58**, 83–95 (2002)
7. Verijenko, V.E., Adali, S., Tabakov, P.Y.: Stress distribution in continuously heterogeneous thick laminated pressure vessels. Compos. Struct. **54**, 371–377 (2001)
8. Xia, M., Takayanagi, H., Kemmochi, K.: Bending behavior of filament-wound fiber-reinforced sandwich pipes. Compos. Struct. **56**, 201–210 (2002)
9. Stroh, A.N.: Dislocations and cracks in anisotropic elasticity. Philos. Mag. **3**, 625–646 (1958)
10. Ting, T.C.T.: Anisotropic Elasticity: Theory and Applications. Oxford Science Publications, New York (1996)
11. Kollár, L.P., Springer, G.S.: Stress analysis of anisotropic laminated cylinders and cylindrical segments. Int. J. Solids Struct. **29**, 1499–1517 (1992)
12. Kollár, L.P., Patterson, J.M., Springer, G.S.: Composite cylinders subjected to hygrothermal and mechanical loads. Int. J. Solids Struct. **29**, 1519–1534 (1992)
13. Bhaskar, K., Varadan, T.K.: Exact elasticity solution for laminated anisotropic cylindrical shells. J. Appl. Mech. ASME **60**, 41–47 (1993)
14. Xia, M., Takayanagi, H., Kemmochi, K.: Analysis of multi-layered filament-wound composite pipes under internal pressure. Compos. Struct. **53**, 483–491 (2001)
15. Xia, M., Kemmochi, K., Takayanagi, H.: Analysis of filament-wound fiber-reinforced sandwich pipe under combined internal pressure and thermomechanical loading. Compos. Struct. **51**, 273–283 (2001)
16. Bakaiyan, H., Hosseini, H., Ameri, E.: Analysis of multi-layered filament-wound composite pipes under combined internal pressure and thermomechanical loading with thermal variations. Compos. Struct. **88**, 532–541 (2009)
17. Calhoglu, H., Ergun, E., Demirdag, O.: Stress analysis of filament-wound composite cylinders under combined internal pressure and thermal loading. Adv. Compos. Lett. **17**, 13–21 (2008)
18. Tarn, J.Q., Wang, Y.M.: Laminated composite tubes under extension, torsion, bending, shearing and pressuring: a state space approach. Int. J. Solids Struct. **38**, 9053–9075 (2001)
19. Tarn, J.Q.: A state space formalism for anisotropic elasticity. Part II: cylindrical anisotropy. Int. J. Solids Struct. **39**, 5157–5172 (2002)
20. Panda, S.C., Natarajan, R.: Finite element analysis of laminated composite plates. Int. J. Numer. Methods Eng. **14**, 69–79 (1979)
21. Karan, S.S., Sorem, R.M.: Curved shell elements based on hierarchical p-approximation in the thickness direction for linear static analysis of laminated composites. Int. J. Numer. Methods Eng. **29**, 1391–1420 (1990)
22. Buragohain, D.N., Ravichandran, P.K.: Modified 3-dimensional finite-element for general and composite shells. Comput. Struct. **51**, 289–298 (1994)
23. ABAQUS Analysis User's Manual, Version 6.11 (2011)
24. Lomakin, E.V.: Torsion of cylindrical bodies with varying strain properties. Mech. Solids **43**, 502–511 (2008)
25. Babuška, I.: Homogenization approach in engineering. Lect. Notes Econ. Math. Syst. **134**, 137–153 (1976)
26. Sanchez-Palencia, E.: Homogenization method for the study of composite media. Lect. Notes Math. **985**, 192–214 (1983)
27. Sanchez-Palencia, E.: Homogenization in mechanics. A survey of solved and open problems. Rend. Sem. Mat. Univ. Politec. Torino **44**, 1–45 (1986)
28. Hashin, Z.: Analysis of composite materials—a survey. J. Appl. Mech. ASME **50**, 481–505 (1983)
29. Charalambakis, N.: Homogenization techniques and micromechanics. A survey and perspectives. Appl. Mech. Rev. **63**, 030803-1–10 (2010)
30. Enie, R.B., Rizzo, R.R.: Three-dimensional laminate moduli. J. Compos. Mater. **14**, 150–154 (1970)
31. Pagano, N.J.: Exact moduli of anisotropic laminates. In: Sendeckyj, G.P. (ed.) Mechanics of Composite Materials, pp. 23–44. Academic Press, New York (1974)
32. Sun, C.T., Li, S.: Three-dimensional effective elastic constants for thick laminates. J. Compos. Mater. **22**, 629–639 (1988)
33. Chen, H.J., Tsai, S.W.: Three-dimensional effective moduli of symmetric laminates. J. Compos. Mater. **30**, 906–917 (1996)
34. Sun, X.S., Chen, Y., Tan, V.B.C., Jaiman, R.K., Tay, T.E.: Homogenization and stress analysis of multi-layered composite offshore production risers. J. Appl. Mech. Trans. ASME **81**, 031003 (2013). doi:10.1115/1.4024695
35. Soden, P.D., Hinton, M.J., Kaddour, A.S.: Lamina properties, lay-up configurations and loading conditions for a range of fibre-reinforced composite laminates. Compos. Sci. Technol. **58**, 1011–1022 (1998)
36. Chen, Y., Tan, L.B., Jaiman, R.K., Sun, X.S., Tay T.E., Tan, V.B.C.: Global-local analysis of a full-scale composite riser during vortex-induced vibration. In: Proceedings of the 32nd International Conference on Offshore Mechanics and Arctic Engineering (OMAE 2013), OMAE2013-11632 (2013)